

AD-A171 884

THE USE OF NOVEL PROCESSING PROCEDURES FOR IMPROVING  
OVERALL FATIGUE RESI. (U) VIRGINIA UNIV CHARLOTTESVILLE  
DEPT OF MATERIALS SCIENCE E A STARKE 28 MAY 84

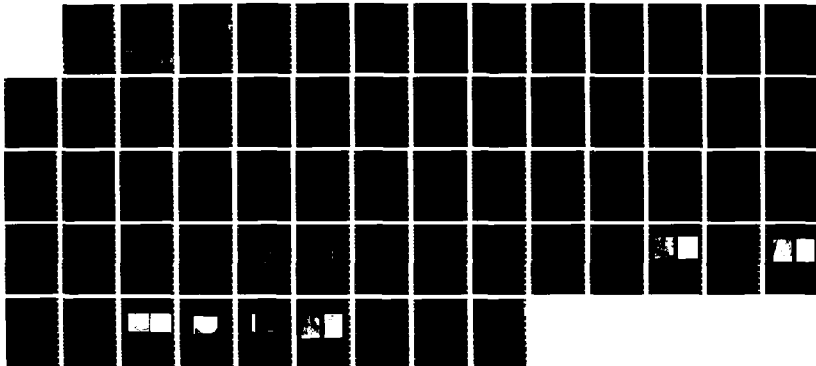
1/1

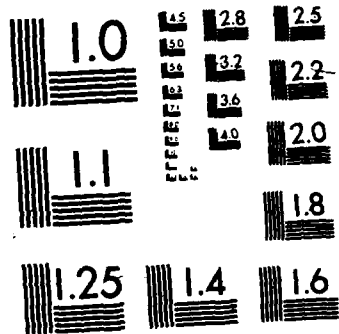
UNCLASSIFIED

UVA/525643/MS85/101 AFOSR-TR-86-0627

F/G 11/6

NL





AFOSR-TR-86-0627

2

AD-A171 884

Annual Report

THE USE OF NOVEL PROCESSING PROCEDURES FOR IMPROVING OVERALL FATIGUE RESISTANCE OF HIGH STRENGTH ALUMINUM ALLOYS

Contract No. AFOSR-83-0061-B

Submitted to:

Air Force Office of Scientific Research/NE  
Building 410  
Bolling Air Force Base  
Washington, D.C. 20332

Attention: Alan H. Rosenstein

Submitted by:

Edgar A. Starke, Jr.  
Professor

AIR FORCE OFFICE OF SCIENTIFIC RESEARCH (AFOSR)  
OFFICE OF TRANSMITTAL TO DTIC  
This technical report has been reviewed and is  
approved for public release IAW AFR 190-12.  
Distribution is unlimited.  
MATTHEW J. REPPER  
Chief, Technical Information Division

Approved for public release ;  
distribution unlimited.

Report No. UVA/525643/MS85/101

May 1985



SCHOOL OF ENGINEERING AND  
APPLIED SCIENCE

DEPARTMENT OF MATERIALS SCIENCE

UNIVERSITY OF VIRGINIA

CHARLOTTESVILLE, VIRGINIA 22901

DTIC FILE COPY

DTIC  
ELECTE  
SEP 15 1986  
S A D

86 9 15 147

2

REPORT DOCUMENTATION PAGE

1a. REPORT SECURITY CLASSIFICATION Unclassified		1b. RESTRICTIVE MARKINGS									
2a. SECURITY CLASSIFICATION AUTHORITY		3. DISTRIBUTION/AVAILABILITY OF REPORT  Unlimited									
2b. DECLASSIFICATION/DOWNGRADING SCHEDULE											
4. PERFORMING ORGANIZATION REPORT NUMBER(S)  UVA/525643/MS85/101		5. MONITORING ORGANIZATION REPORT NUMBER(S)  <b>AFOSR-TR. 86-0627</b>									
6a. NAME OF PERFORMING ORGANIZATION Dept. of Materials Science	6b. OFFICE SYMBOL (If applicable)	7a. NAME OF MONITORING ORGANIZATION Air Force Office of Scientific Research Directorate Electronics & Solid State Sci.									
6c. ADDRESS (City, State and ZIP Code) University of Virginia, Thornton Hall Charlottesville, VA 22901		7b. ADDRESS (City, State and ZIP Code) Bolling, AFB (NE) Washington, DC 20332									
8a. NAME OF FUNDING/SPONSORING ORGANIZATION Air Force Office of Scientific Research	8b. OFFICE SYMBOL (If applicable) <b>NE</b>	9. PROCUREMENT INSTRUMENT IDENTIFICATION NUMBER Grant No. AFOSR-83-0061-B									
8c. ADDRESS (City, State and ZIP Code) Building 410 Bolling AFB, Washington D.C. 20332		10. SOURCE OF FUNDING NOS. <table border="1"> <tr> <th>PROGRAM ELEMENT NO.</th> <th>PROJECT NO.</th> <th>TASK NO.</th> <th>WORK UNIT NO.</th> </tr> <tr> <td><b>61102P</b></td> <td>2306</td> <td>A1</td> <td></td> </tr> </table>		PROGRAM ELEMENT NO.	PROJECT NO.	TASK NO.	WORK UNIT NO.	<b>61102P</b>	2306	A1	
PROGRAM ELEMENT NO.	PROJECT NO.	TASK NO.	WORK UNIT NO.								
<b>61102P</b>	2306	A1									
11. TITLE (Include Security Classification) Use of Novel Processing Procedures...											
12. PERSONAL AUTHOR(S) E. A. Starke, Jr.											
13a. TYPE OF REPORT Annual	13b. TIME COVERED FROM <u>1/1/84</u> TO <u>12/31/84</u>	14. DATE OF REPORT (Yr., Mo., Day) 1984, May, 28	15. PAGE COUNT 55								
16. SUPPLEMENTARY NOTATION											
17. COSATI CODES <table border="1"> <tr> <th>FIELD</th> <th>GROUP</th> <th>SUB. GR.</th> </tr> <tr> <td></td> <td></td> <td></td> </tr> </table>		FIELD	GROUP	SUB. GR.				18. SUBJECT TERMS (Continue on reverse if necessary and identify by block number)			
FIELD	GROUP	SUB. GR.									
19. ABSTRACT (Continue on reverse if necessary and identify by block number) <p>This program was initiated on January 1, 1983. Its objective is to develop an understanding of the mechanisms involved in the initiation and propagation of fatigue cracks in metals in order to optimize the microstructure of high strength aluminum alloys for overall fatigue resistance. The research conducted during this year was divided into three tasks.</p> <p>Task I was concerned with the effects of slip character and grain size on the intrinsic material and extrinsic closure contributions to fatigue crack growth resistance of 7475. It involved the use of thermomechanical processing to modify the grain structure for enhancement of both intrinsic and extrinsic effects. In our last report we described the effect of precipitate type and grain size on fatigue crack growth of 7475 in both vacuum and laboratory. This study showed a very pronounced effect of environment on the fatigue crack propagation behavior. The largest effect was found for an underaged, large grain size version of 7475</p>											
20. DISTRIBUTION/AVAILABILITY OF ABSTRACT UNCLASSIFIED/UNLIMITED <input checked="" type="checkbox"/> SAME AS RPT. <input type="checkbox"/> DTIC USERS <input type="checkbox"/>		21. ABSTRACT SECURITY CLASSIFICATION Unclassified									
22a. NAME OF RESPONSIBLE INDIVIDUAL <b>Mr Ivan Caplan</b>		22b. TELEPHONE NUMBER (Include Area Code) <b>202/767-4934</b>	22c. OFFICE SYMBOL <b>AFOSR/NE</b>								

DTIC  
LECTE  
SEP 15 1986

19. Abstract (continued)

achieved by intermediate thermomechanical treatment. Changing the environment from laboratory air to vacuum resulted in about a 1000X lower fatigue crack growth rate. This dramatic difference could not be explained in terms of state of the art models on crack closure or crack deflection, indicating that a very powerful mechanism is at work which could not be uniquely identified. Two conceivable mechanisms were proposed; (i) increased slip reversibility in vacuum and (ii) possible welding of the fracture surfaces during the unloading part of the fatigue cycle. In order to gain further information on possible mechanisms, a direct current potential drop technique (DC-PD) was installed during the past year to examine the possibility of crack tip welding in vacuum. The results of our initial experiments will be described in the body of the report.

Task II was concerned with a study of the fatigue crack growth and fracture mechanisms of an Al-Li-Cu alloy. Aircraft designers are constantly striving to achieve minimum weight in order to cut fuel consumption and improve overall performance. Reducing the density of structural materials has been shown to be the most efficient solution to this problem. Since aluminum alloys make up between seventy and eighty percent of the current aircraft weight, recent alloy development programs have focused on reducing the density of these materials. Lithium additions to aluminum provide the greatest reduction in density of any alloying element and offer the additional advantage of increasing the elastic modulus. However, Al-Li-X alloys often exhibit low ductility and fracture toughness. Ways of combating this problem have included composition modifications and special thermomechanical processing. During the past year we have studied the fatigue crack growth and fracture toughness behavior of an Al-Li-Cu alloy in order to identify those microstructural features which are beneficial and those which are detrimental. Once these have been identified fracture resistance may be enhanced by microstructure control through special processing. We have found that the fracture toughness is very sensitive to the strain hardening exponent and this parameter can be controlled to some extent by heat treatment.

Task III was concerned with the effect of surface modification on the fatigue crack initiation resistance of 7475 and 2219. Since fatigue crack initiation is a surface phenomenon and fatigue crack propagation is a bulk phenomenon, the fatigue properties may be optimized by production processes that develop microstructures resistant to FCI on the surface, and microstructures resistant to FCP throughout the bulk. We have shown that implantation of Fe into pure aluminum and 7475 produces a fine dispersion of  $Al_6Fe$  particles near the surface. The effect of this dispersion on the FCI of commercially processed and thermomechanically processed 7475 was studied during this year. Experiments on the commercially processed 7475 showed that implantation has a significant effect on the cyclic stress-strain response, increasing the plateau stress and strain dramatically. In the work with ITMT 7475, no such difference was observed. An improvement in FCI resistance was observed for the commercially processed material but not for the ITMT processed material. The lack of improvement for the ITMT alloy was due to the FCI mechanism being associated with grain boundaries in both the unimplanted and implanted conditions, and the lack of effect that the  $Al_6Fe$  precipitates have on grain boundary fracture.

The studies on the effectiveness and feasibility of rapid surface melting and self-quenching of 2219 aluminum alloy using a continuous wave  $CO_2$  laser have begun. Here the goals are to obtain a surface layer free of large constituent particles and, if possible, a considerably hardened layer as compared to the bulk, in order to enhance the resistance to FCI.

Annual Report

THE USE OF NOVEL PROCESSING PROCEDURES FOR  
IMPROVING OVERALL FATIGUE RESISTANCE OF  
HIGH STRENGTH ALUMINUM ALLOYS

Contract No. AFOSR-83-0061-B

Submitted to:

Air Force Office of Scientific Research/Ne  
Building 410  
Bolling Air Force Base  
Washington, D.C. 20332

Attention: Alan H. Rosenstein

Submitted by:

Edgar A. Starke, Jr.  
Professor

Department of Materials Science  
SCHOOL OF ENGINEERING AND APPLIED SCIENCE  
UNIVERSITY OF VIRGINIA  
CHARLOTTESVILLE, VIRGINIA

Report No. UVA/525643/MS85/101  
May 1985

Copy No. \_\_\_\_\_

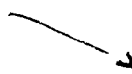
## TABLE OF CONTENTS

	<u>Page</u>
INTRODUCTION .....	1
SUMMARY OF PROGRESS DURING 1984 .....	2
A. The Effect of Microstructure and Environment on Fatigue Crack Propagation of 7475 .....	2
B. Fatigue Crack Growth and Fracture Toughness Behavior of an Al-Li-Cu Alloy .....	7
C. The Effect of Surface Modification on the Fatigue Crack Initiation Resistance of 7475 and 2219 .....	24
PROFESSIONAL PERSONNEL .....	31
GRADUATE STUDENTS .....	31
PRESENTATIONS AND PUBLICATIONS UNDER AFOSR-83-0061 .....	31
REFERENCES .....	32
FIGURES .....	35



Accession For	
NTIS GRA&I	<input checked="" type="checkbox"/>
DTIC TAB	<input type="checkbox"/>
Unannounced	<input type="checkbox"/>
Justification	
BY- _____	
Distribution/	
Availability Codes	
Dist	Avail and/or
	Special
A1	

## I. INTRODUCTION



Recent studies by the Air Force have shown that 50% of all material failures in aircraft are a result of fatigue (1). This high incidence of failures prompted the new safe-crack-growth approach for the design of new aerospace structural systems. However, accurate calculations require a knowledge of fatigue crack growth behavior under a wide variety of load and environmental conditions. Consequently, understanding the mechanisms involved in the initiation and propagation of fatigue cracks in metals is one of the key factors in designing aircraft that are safe, efficient, and economical. Since fatigue crack initiation is a surface phenomenon and fatigue crack propagation is a bulk phenomenon, the fatigue properties may be optimized by production processes that develop the desired microstructures for FCI resistance on the surface, and the desired microstructure for FCP resistance throughout the bulk. The objective of this program is to optimize the microstructure of high strength aluminum alloys for overall fatigue resistance, i.e., resistance to both FCI and FCP, through the use of new primary processing methods. Specifically, this research will identify those microstructural features that control the different aspects of fatigue, and establish methods for incorporating those features in a finished product.



## II. SUMMARY OF PROGRESS DURING 1984

### A. The Effect of Microstructure and Environment on Fatigue Crack Propagation of 7475

The purpose of this study was to investigate the roughness induced and oxide-induced crack closure behavior of 7475 aluminum alloy under different microstructural and environmental conditions. Emphasis was placed on the effect of grain size and deformation mode on crack closure of compact tension samples subjected to plane strain conditions in a vacuum and in a laboratory air environment. In our last report we reported that there was a very pronounced effect of environment on the fatigue crack propagation behavior in an underaged, large grain size version of 7475 that had been produced using intermediate thermomechanical processing. The 1000X difference in fatigue crack growth rates that was observed between vacuum and laboratory air could not be explained in terms of state of the art models on crack closure or crack deflection. Two conceivable mechanisms were proposed by us in the paper that was published on that research, (i) increased slip reversibility in vacuum and (ii) possible welding of the fracture surfaces during the unloading part of the fatigue cycle (2). During the past year we have used a direct current potential drop technique in an attempt to clarify the mechanism involved.

The PD method is based on the increase in electrical resistivity with increasing crack length. Figure 1 shows the locations where direct current is fed into the CT-specimens and where the potential drop is measured. The actual current input is through brass screws and the voltage is measured with the help of spotwelded copper wires.

A highly stable Sorensen SRL 10-50 power supply and an ultrasensitive Hewlett Packard 3456 A digital voltmeter are used in this setup. An HP85 desk computer is interfaced to the HP3456 A voltmeter and a Keithley 195A digital multimeter which carries the load signal. This arrangement allows the recording of applied load and associated potential drop voltage. The potential drop voltage was related to crack length by comparison with calibration tests run previously on dummy aluminum samples for which the crack length was monitored with a travelling optical microscope in addition to the PD method. The resulting calibration curve is shown in figure 2. Plotted is reduced cracklength  $\frac{a}{w}$  (cracklength divided by sample width) versus reduced potential drop voltage  $\frac{V}{V_0}$  (voltage divided by the voltage at  $\frac{a}{w} = 0.5$ ). Because of the low electrical resistivity of aluminum a direct current of 50 amperes had to be passed through the sample in order to achieve good resolution. Voltages were measured typically in the range of 0.3 to 1.5 mV.

The material used was received as commercially available 7475 1.2" thick plate in the T7351 temper. Intermediate thermomechanical treatment was applied to achieve a large grain version (80  $\mu$ m) in the way described by Carter et al. (2). After solution heat treatment and stretch (2%), compact tension specimens were machined with the loading line parallel to the rolling direction. Samples were underaged (6 hrs. @ 120°) and overaged (17 hrs @ 160°). Due to the limited amount of material only 2 CT specimens of each heat treatment could be obtained.

The mechanical tests were performed on a closed loop servo-hydraulic MTS machine, at room temperature, an R-ratio of 0.1, and a frequency of 30 Hz. Crack length was monitored with a travelling

microscope and the DC-PD method. Crack closure was measured with back face strain gages at about 0.1 Hz. At the same time the compliance curve was taken, load and associated potential drop voltage were recorded by the HP 85 computer for later plotting.

Precracking was done while the environmental chamber was filled with laboratory air. The constant current through the sample didn't result in any increase of its temperature in air. In vacuum, however, a temperature of 80° C was measured on dummy samples because of lacking heat transfer to surrounding air. In order to run the experiments at room temperature heat transfer to a surrounding medium is necessary. For that reason the environmental chamber was filled with high purity argon after it passed through a Centorr 2 B-20-Q gettering furnace which contained hot titanium where oxygen, nitrogen and water were removed. The purified argon atmosphere was believed to have about the same low partial pressure of oxygen as in high vacuum. No increase in sample temperature could be detected in argon.

#### Results and Discussion

Figure 3 shows the fatigue and propagation results (argon) compared with our earlier data subsequently referred to as Carter's. Two samples of each aging condition were tested. The overaged data in argon coincide with the overaged data in vacuum (Carter). The underaged alloy, however, shows much higher propagation rates in argon than in vacuum and at high  $\Delta K$  values only a small difference in crack propagation rates exists between the two aging conditions. The dramatic difference in propagation rates in vacuum could not be verified with the experiments in argon atmosphere. Crack closure occurred in both aging treatments and in contrast to Carter's vacuum data, where

there was a larger amount of closure in the underaged condition at any  $\Delta K$ , the same amount of closure was measured for the two aging conditions in argon. Figure 4 shows the difference in closure behavior for vacuum and argon samples. Below a  $\Delta K$  of 7 MPa  $\sqrt{m}$  the argon samples show less closure than either the underaged or overaged samples in vacuum. At  $\Delta K$  levels above 7 the argon data indicate more closure than in the overaged vacuum experiments. The highest amount of closure is still measured from underaged samples in vacuum. At around  $\Delta K \sim 11$  MPa  $\sqrt{m}$  crack closure is close to zero for all experiments. Closure caused by plasticity is not believed to contribute much at these fairly low  $\Delta K$  levels. Assuming the absence of oxide induced closure in the argon atmosphere, closure is most likely associated with microstructural asperities and fracture surface roughness.

Figure 5a and b are optical micrographs of the fatigue crack paths of the argon samples which are also an indication for the fracture surface roughness parameter. The fracture surface of the underaged alloy was much rougher than for the overaged sample tested in vacuum. Carter's micrographs show a distinct difference in crack path between under- and overaged conditions. The crack profiles in argon look very much like the overaged ones in vacuum reported by Carter. If one compares overaged and underaged aluminum alloys, a more tortuous crack path and crack branching in underaged conditions together with associated higher slip reversibility and mode II components in crack opening generally exhibit lower fatigue crack growth rates. From that viewpoint it is not surprising that the same crack path and fracture

surface roughness for the two aging treatments in argon result in almost the same crack propagation behavior.

The higher propagation rates for the underaged samples in argon compared to vacuum may be partially attributed to the lack of these beneficial features. The argon atmosphere seems to contain enough impurities, like oxygen, hydrogen and/or water vapor, that a high degree of slip reversibility, as is found in good vacuum, couldn't be achieved. Typically underaged conditions exhibit more localized slip than their overaged counterparts which makes the former more susceptible to localized diffusion of species such as oxygen or hydrogen into the process zone ahead of the crack tip. For that reason underaged aluminum alloys are much more sensitive to environmental changes than overaged ones. Apparently the purified argon was clean enough for the overaged samples which is demonstrated by the almost identical FCP curves in argon and vacuum. For the underaged condition this is not the case.

Figure 6 shows the crack growth data after correcting for crack closure. Because the amount of closure for both conditions tested in argon were the same, these curves don't shift with respect to each other. The fatigue crack growth resistance of the underaged condition in vacuum is still about two orders of magnitude higher. Whatever mechanism is responsible for these low propagation rates, it is not present in the argon atmosphere.

Plotting of applied load versus potential drop voltage should indicate the presence of fracture surface welding because the voltage signal is very sensitive to changes in crack length. Figure 7 shows a representative plot where the sample has been loaded and unloaded with

a ramp at ~0.1 Hz. The voltage is independent of the load applied to the sample, i.e., no change in crack length occurred during this loading cycle. No welding has been detected by this method in any of our experiments in argon. Fracture surface welding is usually harder to get in gaseous atmosphere than in vacuum.

#### Further Research

Evidently the high purity argon atmosphere is not clean enough to be compared to vacuum. For that reason fatigue crack propagation experiments will be performed in ultra high purity argon which additionally will be cleaned in a gettering furnace. If this environment will not produce vacuum-like crack propagation rates in the underaged samples the potential drop setup needs to be modified so it can be used in vacuum without heating up the sample. The principle of this modification will be the utilization of direct current pulses instead of permanent current input. This way the temperature may only increase slightly. The powerful tool of the DC-PD technique can then be used to get a close-look at the reasons why the underaged alloy exhibits such extremely low propagation rates in vacuum.

#### B. Fatigue Crack Growth and Fracture Toughness Behavior of an Al-Li-Cu Alloy

The goals of most Al-Li-X alloy development programs include improvements in density and modulus with equivalent or improved damage tolerance and corrosion properties compared with currently used materials, e.g., 7075 and 2024 (3). Although there have been numerous reports on the relationship between composition, microstructure and monotonic properties of Al-Li-X alloys (4,5), there

have been few studies on the cyclic properties and fracture toughness of these materials. This task was concerned with the fatigue crack propagation and fracture toughness of a new alloy based on the Al-Li-Cu system which is somewhat related to the Al-Li-Cu alloy 2020 that was commercially available in the 1960's.

The chemical composition of the Al-Li-Cu alloy used for the study is shown in Table 1. It is similar in composition to the Al-Li-Cu alloy, M2, recently studied by Feng et al. (6), except for slightly lower copper and cadmium and slightly higher lithium contents. In addition to the above, low levels of Fe and Si were maintained to minimize the amount of constituent phases. Zirconium was added as the dispersoid forming element.

TABLE 1  
Chemical Compositions in weight percent

Cu	Li	Cd	Zr	Fe	Si	Al
3.6	1.68	0.16	0.16	0.01	0.02	bal.

The material was obtained from Reynolds Metals Company in the form of 27.7 mm thick plates. The original cast ingots were homogenized in an argon atmosphere as follows: (i). Heated at 523 K/hour to 673 K, held 48 hours, (ii). heated at 298 K/hour to 763 K, held 18 hours and (iii). heated at 298 K/hour to 788 K held for 30 minutes and fan cooled. The ingots were scalped on the surface to 69.8 mm thick and then cleaned. The hot rolling was performed in three steps, preheated to 733 K, held for one hour, hot rolled from 69.8 mm to 57.1 mm, reheated to 733 K, hot rolled to 44.5 mm, reheated to 671 K and hot rolled to a final thickness of 27.7 mm.

The alloy was solutionized in a salt bath at 788 K for 30 minutes, quenched in ice water, stretched 2 percent and aged in an oil bath at 433 K for different periods of time. Fracture toughness was measured on 11 mm thick compact tension samples in the L-T orientation and a conditional  $K_{1c}$  value for fracture toughness was obtained from the load-crack opening displacement plots by choosing the 5 percent secant offset line. Of all the samples tested only the two underaged samples did not meet the ASTM thickness criterion,  $b \geq 2.5(K_{1c}/\sigma_{ys})^2$ . A thickness of 54 mm would have been required for the underaged samples for a valid  $K_{1c}$  test.

Crack propagation tests were conducted on compact tension specimens in laboratory air (R.H. ~45 percent) and a vacuum of  $10^{-5}$  torr at 295 K using an R ratio of 0.1 and a frequency of 30 Hz. The crack propagated in the long transverse direction on a plane normal to the rolling direction. Crack growth monitored with a travelling microscope and load versus crack opening displacement curves were generated by the elastic compliance techniques. Near threshold crack growth rates were obtained by the load-shedding scheme. At every load level the crack was allowed to propagate a distance equal to at least three times the cyclic plastic zone size and then the load was decreased by three percent.

The microstructures were examined by optical, scanning and transmission electron microscopy. The foils for transmission work were obtained with a dual jet Tenupol apparatus by using fifty percent nitric acid-methanol mixture at 253 K and a potential difference of 15 volts. Fracture surfaces were examined with a scanning electron microscope.

## Results and Discussion

### Microstructure and Tensile Properties

Optical metallography revealed a predominantly unrecrystallized structure in the as-rolled condition with large elongated unrecrystallized grains. However, some recrystallization occurred during solution treatment. A high degree of recrystallization has been shown to be undesirable in Al-Li-X alloys since secondary crack paths are invariably associated with recrystallized grains (7). Thus from a ductility point of view, it is advantageous to select a low solutionization temperature in order to suppress recrystallization (7). However, if the temperature is too low, some strength is lost due to incomplete solutionizing prior to aging. In the present work a solution treatment temperature of 788 K was found to be an optimum temperature to achieve the desired strength level, while minimizing the degree of recrystallization.

TEM studies revealed subgrains with an average diameter of 5 microns. The major strengthening precipitates were identified as  $\theta'$ (Al<sub>2</sub>Cu), and T<sub>1</sub>(Al<sub>2</sub>CuLi). The tensile properties obtained at various aging times are listed in Table 2. The peak strength was found to be lower than that of the M2-T651 alloy investigated by Feng et al. (6). This is attributed to the lower Cu content in the present alloy and thus a lower volume fraction of the major strengthening precipitates,  $\theta'$  and T<sub>1</sub>.

TABLE 2

Aging time	$\sigma_{ys}$	$\sigma_{uts}$	percent elongation	n	K <sub>1c</sub>
8	300	431	20	0.13	44
12	350	452	18	0.098	40
17	520	534	8	0.055	32.2
19	500	526	8.6	0.062	30
22	484	500	6.6	0.056	27
26	472	496	4.0	0.062	30

The slip behavior was studied by TEM analysis of thin foils obtained from regions adjacent to the fracture surface of the tensile samples. In the as-quenched condition only a few planar slip bands were observed at near fracture strain and only in certain grains as most of the deformation was homogeneously distributed. These slip bands may be associated with some  $Al_3Li(\delta')$  being present in the as quenched condition. With progressive aging the fine relatively homogeneous slip changed to well-defined intense slip bands in the peakaged condition. These bands became more prominent, the separation between them increased, and their width decreased as aging progressed. The slip bands persisted in the slightly overaged condition, due to the presence of coherent and partially coherent precipitates. However, they were more diffused when compared to the peakaged condition suggesting a slight reversal to relatively homogeneous slip. The slip bands were most often contiguous across the subgrains.

The changes in the monotonic properties and slip behavior with aging show that the increase in the yield strength is accompanied by increasing amounts of strain localization in the slip bands and a concomitant decrease in the strain hardening exponent and ductility level. Similar behavior has been observed in the past by Sanders and Starke (8) in Al-Li binary alloys, Ludtka and Laughlin (9) in 7475 alloy with different Mg additions and Hornbogen and Zum Gahr (10) in Fe-Ni-Al alloy for different aging conditions.

The model developed by Gleiter and Hornbogen (11,12) to describe dislocation shearing of misfit-free ordered particles may be applied to the present results. This model essentially states that the increase is

in the critical resolved shear stress,  $\Delta\tau_0$ , associated with the strengthening precipitates is proportional to the product of their volume fraction,  $f$ , and their radius  $r_0$ , given by

$$\Delta\tau_0 = 0.28 G^{-1/2} b^{-2} \nu^{3/2} f^{1/2} r_0^{1/2} \quad [1]$$

where  $\nu$  is the antiphase boundary energy,  $G$  is the shear modulus and  $b$  is the Burgers vector. The increase in the strength of this alloy with aging qualitatively conforms to this model since both the volume fraction and radius of the precipitates would increase with aging. Furthermore, the present experimental results of slip behavior and previous observations on Al-Li alloys (8) indicate that the degree of work softening increases with  $f^{1/2} r_0^{1/2}$ . Due to the complexity of the alloy no quantitative measurements of the volume fractions, diameter, and coherency of the strengthening precipitates have been made.

The lower degree of strain localization associated with the underaged conditions results in a larger capacity for strain accumulation. This is reflected both by the high strain hardening exponents and strains to fracture. With aging the strain hardening exponents decrease due to the easier movement of the dislocations in the slip bands (8), and since the majority of the deformation is localized, the net effect is a lower ductility level. Beyond the peakaged condition, when the particle radius increases the coherency of  $\theta'$  and  $T_1$  is lost, there is a slight tendency for the strain hardening exponent to rise as the dislocations by-pass the particles and more homogenous slip occurs. Although planar slip bands were prevalent in this aging condition homogenous slip was observed in between the slip bands.

Transgranular shear fracture was observed for both the underaged and overaged alloys along with some voids associated with the precipitate particles or slip band intersections. There was little evidence of intersubgranular fracture and voids associated with large equilibrium precipitates along the subgrain boundaries. TEM examination of a sample aged for 22 hours revealed extremely long slip bands due to only a slight misorientation of the subgrains. Thus, the transfer of plasticity to adjacent subgrains is easily attained and this minimizes intersubgranular cracking. However, as discussed later, the intersubgranular ductile fracture processes were more prevalent in the notched fracture toughness samples. The ductile intergranular cracking associated with the equilibrium precipitates was often observed in the overaged condition. Intense secondary cracking was observed and may be associated with the small recrystallized grains, but is most likely due to the presence of coarse equilibrium precipitate observed at the high angle grain boundaries. The decrease in ductility with aging seems to be simply due to the extensive shear localization and accompanying slip band softening up to the peakaged condition. Beyond the peakaged condition larger equilibrium precipitates on the grain boundaries give rise to intergranular cracking which further reduces the ductility.

#### Fatigue Crack Propagation

The results obtained from the fatigue crack propagation tests in air (R.H. 45 percent) and in vacuum ( $<10^{-5}$  torr) are shown in Figures 8 (a) and (b) as plots of crack propagation rates  $da/dN$  versus the stress intensity factor range  $\Delta K$ . The near threshold fatigue crack growth rates increased and the threshold stress intensities (Table 3) decreased with aging in both air and vacuum. Furthermore, there is

an enhancement of the fatigue crack growth resistance in vacuum for similar aging conditions. The crack closure data obtained from the compliance versus load curves has been expressed (13) in the form of the closure stress intensity factor  $\Delta K_{th}^{Cl} = K_{th}^{Cl} - K_{th}^{min}$  and the intrinsic (or effective) stress intensity factor  $\Delta K_{th}^i = \Delta K_{th}^{obs} - \Delta K_{th}^{Cl}$ , as shown in Table 3. These values indicate that the intrinsic fatigue crack growth thresholds follow the same trend as the apparent or observed values, for the aging conditions tested here.

TABLE 3  
Fatigue Threshold Stress Intensities

Condition	Environment	$\Delta K_{th}$ Mpa <sup>1/2</sup>	$\Delta K_{th}^i$ Mpa m <sup>1/2</sup>	$\Delta K_{th}^{Cl}$ Mpa m <sup>1/2</sup>
UA	Air	3.7	3.1	0.6
PA	Air	2.8	2.4	0.4
OA	Air	2.3	2.3	negligible
UA	Vacuum	5.5	5.3	0.2
PA	Vacuum	4.3	4.0	0.3

$$\Delta K_{th} = \Delta K_{th}^{observed} \text{ or } \Delta K_{th}^{apparent}$$

$$\Delta K_{th}^i = \Delta K_{th} - \Delta K_{th}^{Cl}$$

$$\Delta K_{th}^{Cl} = K_{th}^{Cl} - K_{th}^{min}$$

Figure 9, shows the crack paths for the alloy tested in the air in the under and overaged conditions. The observed deflections appear to be due to the crack propagating along the slip bands. It is not surprising that extensive crack deflections occur in the overaged alloy since slip planarity is maintained and intense slip bands are available for crack propagation paths.

Figure 10 compares the results obtained for the Al-Cu-Li alloy with those of the thermomechanically processed 7475 as Carter described in Section II-A. The fatigue crack growth rates and thresholds of the Al-Cu-Li alloy are better than those of the 80  $\mu\text{m}$  grain size 7475. Several investigators have proposed that the fatigue crack growth rates decrease with increasing modulus (14), thus indirectly predicting that Li-containing Al alloys would have improved FCP resistance. Therefore, a more realistic comparison of the two materials may be obtained by normalizing the stress intensity range with Youngs' modulus since the yield stresses are approximately the same. As shown in the normalized curves of Figure 10 (b), the fatigue growth rate curves remain above the 7475 alloy suggesting that the improvement is not due to the modulus effect alone. In a similar comparison, Vasudevan et al. (15) came to the conclusion that the crack deflections in the 2020 alloy were a major cause for improved crack growth resistance over that of a 7075 alloy. A comparison of the crack deflections observed in 7475 (2) with those observed here also show that this mechanism may account for the improved crack growth resistance observed, although differences in slip reversibility may also be a contributing factor.

In the present alloy the crack propagation rates are lower in the underaged condition as compared to the peak and overaged conditions. These observations are consistent with earlier observations made by other investigators in age hardened systems (2,16,17). In these alloys, the dislocations shear the coherent precipitates and thus promote inhomogeneous slip in the underaged condition. In the overaged alloys, the coherency between the precipitates and matrix is reduced resulting in less heterogeneous slip as discussed before. The dislocations emitted

from the crack tip move forward on the slip plane in the rising half of the fatigue cycle and a fraction move in the reverse direction during the falling half of the fatigue cycle. In the underaged condition the fraction of the dislocations that move back is larger compared to the overaged condition since the particles are cut in the former case. In other words, the slip reversibility would be higher in the underaged alloy and the plastic strain accumulation would be lower for a given number of cycles. For the overaged alloys, the slip reversibility is reduced because of the precipitate bypass mechanism and this leads to a higher accumulation of plastic strain for the same number of cycles. This implies that for a given  $\Delta K$  an overaged material would exhibit faster crack growth rates compared with an underaged material. The general observation has been that precipitation hardened alloys show decreasing crack growth resistance with increasing slip homogeneity when other variables are constant. The lowering of the crack rates in the underaged alloy can be directly attributed to the above slip process (2,16,17), since there is no substantial difference in the crack deflections. For the 7475 alloy tested in vacuum, Carter et al. (2), showed that in spite of a major difference in the crack deflections between the under and overaged conditions the contribution from this microgeometrical effect (18) could not account for the overall differences in the crack growth resistance.

Our current results also suggest that the  $\Delta K_{th}^{CI}$  decreases and  $\Delta K_{th}^i$  increases in vacuum. Firstly, the reduction in  $\Delta K_{th}^{CI}$  in vacuum may be due to a decreased propensity for load bearing oxide asperities. Secondly, although a rougher fracture surface or extensive faceting is observed in vacuum, the absence of oxide induced asperities could

substantially decrease the mismatch between crack faces. In laboratory air, a possibility for crack tip oxidation is more likely and if the thickness of the oxide layer is comparable to the crack opening displacement, oxide induced crack closer may occur. Carter et al. (2) proposed that slip reversibility could also increase in vacuum due to less oxide formation. Thus, although the fractography indicates extensive faceting it does not result in an increase of  $\Delta K_{th}^{CI}$  in vacuum. The effects of Mode II displacements behind the crack tip appear to be reduced in vacuum due to improved slip reversibility and the absence of load bearing oxide asperities. Thus intrinsic crack growth resistance,  $\Delta K_{th}^i$ , in vacuum is improved.

#### Fracture Toughness

One of the major goals in the development of Al-Li alloys has been to develop microstructures capable of exhibiting fracture toughness levels comparable to the 7XXX series and improvements in strength, modulus, and density over the existing 2XXX alloys. Although several investigations have addressed the ductility problems of these alloys, very few have concentrated on the problem of fracture toughness. Previous investigations (19,20) on the fracture behavior of the Al-Li-X alloys have shown that strain localization curtails ductility in the peakaged condition. Strain localization, in conjunction with large equilibrium precipitates along boundaries, promote intergranular/intersubgranular fracture associated with wide PFZ's. Efforts to decrease the formation of the PFZ's have included chemistry modifications and deformation prior to aging. The latter process involves the introduction of dislocations which serve as sites for those precipitates that have a large coherency strain field, e.g.,  $\theta'$  and  $T_1$ .

Recent studies by Feng et al. (6) on Al-Li-Cu alloys have shown that in the presence of Cd, deformation prior to aging might not be necessary to obtain a uniform and dense precipitation of the  $\theta'$  and  $T_1$  phases. Another beneficial effect of Cd is to slow down the growth kinetics of the strengthening precipitates by segregating to the  $\theta'$ -matrix interfaces (21,22). However, excessive amounts of Cd may segregate to the grain boundaries and contribute to the intergranular fracture.

Recrystallized and partially recrystallized structures may also be detrimental to ductility when compared with unrecrystallized structures due to secondary crack paths along the recrystallized grains (7). The suppression of recrystallization in aluminum alloys is normally attained by adding dispersoid forming elements, Cr or Mn or Zr. Of these, Zr has been observed to be the most potent in suppressing recrystallization (23). The improvement in the fracture toughness observed when adding Zr has been associated with a lesser degree of secondary cracking along the recrystallized grains (23). However, it may also be associated with the small particle size and coherent interface when compared with Cr and Mn dispersoids. All of these factors may reduce the fracture toughness by enhancing the fracture processes in the presence of a notch. In the present work we have concentrated on the effect of the slip process on the fracture toughness. The slip process is undoubtedly controlled by the strengthening precipitates but eventually the slip dictates the fracture toughness in Al-Li-X alloys as discussed below.

The fracture toughness data collected over a wide range of aging times from compact tension specimens, are summarized in table 2. The

results show decreasing fracture toughness with aging, typical of many other aluminum alloys such as 2020 (24). The accompanying change of yield stress with aging, Figure 11, shows that the  $K_{1C}$  decreases as the yield stress increases until the peakaged condition is attained beyond which the strength toughness combination decreases. A comparison of the  $K_{1C}$  values of this alloy to the commercial 2020 alloy containing Cu, Li, Mn, and Cd (Figure 11) shows that the toughness levels are comparable only at the lower aging condition, whereas for longer aging the present alloy retains high toughness. For example, at a strength level of 475 MPa, the  $K_{1C}$  values are 35 and 20  $\text{MPa}\cdot\text{m}^{\frac{1}{2}}$  for the present alloy and the commercial 2020 alloy, respectively. In the same Figure,  $K_{1C}$  values recently obtained for an Al-2Li-4Mg alloy (24) and a modified 2020 alloy (6) are also shown for comparison purposes.

The other mechanical property data shows that the decreasing fracture toughness is accompanied by a decrease in the strain hardening exponent and strain to fracture suggesting the possible role of these variables on the fracture toughness, as will be discussed later. Extensive fractography of the fracture toughness samples revealed five different fracture processes. These are (i) transgranular shear band failure, (ii) secondary cracking along the recrystallized grains, (iii) voids associated with necking of the subgrains, (iv) some very rare occurrence of transgranular microvoid coalescence, and (v) ductile intergranular failure.

The major mechanism of failure in the under to peakaged conditions is transgranular shear band failure along with secondary cracking associated with recrystallized grains. In many instances failure was found to occur over several microns along the shear bands. These

observations suggest that the slip bands emanating from the crack tip have often extended unimpeded transgranularly across many subgrains and possibly several grains. This is due to the low misorientation between subgrains and the sharp deformation texture of the plate. There was an entire change in the mechanism of fracture for the overaged condition; small microvoids were observed along grain boundaries suggesting a ductile intergranular type of failure, associated with a weakening of the grain boundaries in the overaged condition. Starke, Sanders and Palmer (19) suggest that for Al-Li alloys the slip bands impinging on the grain boundaries transfer the strain to the soft PFZ's along the grain boundaries. These regions deform with ease and hence strain is localized here, giving rise to a more easily attainable fracture route along the grain boundaries.

Many investigations in the past have shown that a relationship between the strain hardening exponent obtained in uniaxial tension tests and  $K_{1C}$  exist (25-27). Recently, Garret and Knott (25) have shown that the critical crack opening displacement at the onset of crack extension is proportional to the square of the strain hardening exponent for a constant ductile fracture strain, thus suggesting that the  $K_{1C}$  is proportional to the strain hardening exponent. Due to the dispersion of the plasticity, the crack tip in the underaged condition experiences a lower strain concentration than in the peakaged condition for a given load level. Thus the load bearing capacity in the presence of a notch is higher in the underaged conditions. If the crack extension took place after a critical strain has accumulated (critical strain criterion) in front of the crack tip (or when the strain hardening capacity is

exhausted) then the underaged samples would exhibit a higher fracture toughness.

The above relationship between the fracture toughness and the strain hardening exponent does not, however, offer an explanation at a microscopic level, since the plastic zones in front of the crack tip include the plasticity in intense slip bands as well as the plasticity between the bands. In order to incorporate microstructural features and/or the process zone it might be necessary to consider the extent of strain localization which is controlled by the character of the strengthening precipitates. Going from the under to the peakaged condition, the fracture toughness is limited by the slip band decohesion process without the involvement of any void growth. Thus with aging, as the strength increases and strain hardening capacity decreases the fracture process could occur due to an increase in the ease of strain localization (28). The extent of the slip localization inherently takes into account the effects of the strain hardening exponent, and the attainment of a critical strain in the slip band before decohesion occurs.

The critical strain for crack extension by transgranular slip band fracture is produced in the plastic zone in front of the crack tip when the crack is opened. The crack opening displacement,  $\delta$ , may be equilibrated to the total number of dislocations,  $n$ , that are emitted from the crack tip during crack opening, times the Burgers vector (29), i.e.,

$$\delta = nb \quad (2)$$

Some of these dislocations may be homogeneously distributed throughout the plastic zone and some may be concentrated in intense slip bands

that lie within the plastic zone. consequently,  $\delta$  may be written as the sum of these contributions,

$$\delta = (n)_u b + (n)_{SB} b \quad (3)$$

where  $(n)_u b$  represents the uniform displacement in the plastic zone and  $(n)_{SB} b$  represents the displacement in the slip bands. The relative magnitude of each contribution would be dependent on the aging conditions since the tendency for strain localization increases as aging progresses up to the peakaged condition. Only those dislocations in the intense slip bands should be considered to contribute to the critical strain that is necessary for transgranular slip-band fracture. The density of these dislocations may be defined as

$$\rho_{SB} = (n)_{SB} / LW \quad (4)$$

where  $W$  is the slip band width and  $L$  the slip band length. Following Orowan, the shear strain in the slip band may be written as

$$\begin{aligned} \gamma_{SB} &= \rho_{SB} bL \\ &= \frac{(n)_{SB}}{LW} \cdot bL = (n)_{SB} b/W \end{aligned} \quad (5)$$

A critical value of  $\gamma_{SB}$  would be necessary for fracture to occur. As aging processes a smaller  $\delta$  is required to reach the critical strain since, for a given  $\delta$ ,  $(n)_{SB}$  increases and  $W$  decreases with aging. We may express  $\delta$  in terms of the stress intensity factor,  $K$ , the yield stress,  $\sigma_{ys}$ , and Youngs' modulus,  $E$ , by the relationship (30)

$$\delta = \frac{K^2}{E\sigma_{ys}} \quad (6)$$

Substituting for  $\delta$  and ignoring the contributions of those dislocations that are homogeneously distributed, we obtain

$$\frac{k^2}{E\sigma_{ys}} = \gamma_{SB} W \quad (7)$$

Initial crack extension occurs when  $\gamma_{SB}$  reaches a critical value,  $\gamma_{SB}^C$ , and the fracture toughness may be expressed as

$$J_{1c} = (E\sigma_{ys} \gamma_{SB}^C W)^{\frac{1}{2}} \quad (8)$$

Although the yield strength increases with aging, thus suggesting an increase in fracture toughness, the yield strength is accompanied by an increase in strain localization and a decrease in  $W$ , which, as equation (8) predicts, decreases the fracture toughness.

It is interesting to note here, that the above equation is similar to the equation 13(c) in reference (31), originally proposed by Ritchie et al. (32) and recently reexamined by Ritchie and Thompson (31). In that equation, the authors proposed that crack initiation occurs when a critical fracture strain  $\epsilon_f^*$ , is attained over a characteristic fracture distance  $l_0^*$  equal to half the distance between void initiating particles.

In the present equation fracture initiation takes place when a critical fracture strain is achieved over a slip band width  $W$  characteristic of the aging condition. The equation proposed here suggests that the precipitates that increase the strength also cause the critical fracture strain to be achieved over a decreasing slip band width resulting in a lower fracture toughness, until the peakaged condition is reached. The fracture mechanism changes after overaging.

The behavior of the newly developed Al-Li-X alloys is different from most other aluminum alloys in that the characteristic fracture associated with void initiation at constituent particles and coarse incoherent Mn and Cr dispersoids and the subsequent void growth by shear localization is absent. The volume fraction and size of these

particles is low due to the extremely low contents of the Fe and Si, Table 1 and the use of Zr as the dispersoid forming element. Previous work (6) on Al-Li-Cu alloys containing higher Fe and Si contents suggest that coarse constituent particles aid in fracture initiation via microvoid nucleation at these particles and curtail ductility. The Cr and Mn dispersoids may homogenize slip in aluminum alloys and thus, increase the work hardening exponent. However, the detrimental nature of the large Mn and Cr containing particles on the fracture ductilities is clearly demonstrated in the literature (23). Microvoids are normally not associated with the small coherent  $Al_3Zr$  dispersoids.

#### C. The Effect of Surface Modification on the Fatigue Crack Initiation Resistance of 7475 and 2219

Since fatigue crack initiation is a surface phenomenon and fatigue crack propagation is a bulk phenomenon, the fatigue properties may be optimized by production processes that develop microstructures resistant to FCI on the surface, and microstructures resistant to FCP throughout the bulk. This task is concerned with the modification of the surface for FCI resistance using both ion implantation and laser processing.

##### Fe Implanted 7475

The underaged, large grained 7475 produced by intermediate thermomechanical processing which showed the best resistance to fatigue crack propagation in the study described in Section II-A was selected for ion implantation. A commercially produced 7475 similarly aged was also studied for comparison purposes. As mentioned previously, the underaged alloy deforms by planar slip which is advantageous to fatigue crack growth resistance, although detrimental to fatigue crack initiation

resistance. Thus by implanting Fe into the ITMT processed 7475 it may be possible to retain a structure resistant to FCP in the bulk while modifying the surface to improve FCI resistance. Fatigue specimens machined from both the commercially processed and ITMT processed 7475 were implanted with  $\text{Fe}^+$  ions at a beam energy of 100 KeV to a dose of  $5 \times 10^20$  ions/m<sup>2</sup>.

Implanted specimens were electrolytically thinned on the unimplanted side for TEM observation. Fig. 13 is a B.F. of the implanted surface. Diffraction analysis shows that the thin plates are  $\text{FeAl}_6$ . Also this micrograph shows an absence of the dispersoid phases found in the bulk structure. The explanation for the precipitation of  $\text{FeAl}_6$  and the dissolution of dispersoid phases during implantation lies in ion beam-specimen interaction. When 100 KeV  $\text{Fe}^+$  ions strike the Al lattice a collision cascade is produced. This results in a local thermal spike (33). According to the theory worked out by Sigmund (33), the temperature of this spike for 100 KeV  $\text{Fe}^+$  into Al is 605 K with a lifetime of about  $10^{-10}$  sec. Previous studies have suggested that precipitation occurs at room temperature after implantation by radiation enhanced diffusion.

However, at an ion beam current of 1 $\mu$ Ampere, an ion would strike the surface every  $10^{-13}$  seconds and at a dosage of  $5 \times 10^{20}$  ions/m<sup>2</sup> it would take 170 min. to implant the specimen. In addition, if precipitation occurred at room temperature, a wide range of ternary compounds would be stable such as  $\text{Al}_7\text{Cu}_2\text{Fe}$ . However, at 635 K (605 K over room temperature),  $\text{Al}_6\text{Fe}$  is the only phase which is stable in this system. Also the apparent dissolution of dispersoid phases of sizes on the order of 0.01  $\mu\text{m}$  is evidence that the system was at a high

temperature for a substantial amount of time. This is not to say that at room temperature the  $Al_6Fe$  particles did not grow by a radiation enhanced diffusion mechanism, but only that they were nucleated during the implantation process.

If precipitation did occur during implantation and not after by radiation enhanced diffusion, changes in ion beam energy should cause different compounds to be stable. For instance, raising the beam energy to 200 KeV would result in a theoretical thermal spike of 300 K in the implanted zone. This could cause different compounds to be stable.

The Coffin-Manson plot of the commercially processed 7475 in Figure 14 shows that the strain life above 0.4% plastic strain amplitude is increased by implantation. However, when the slope changes at lower strain amplitudes, there appears to be no effect. This is most likely because of a change in the site of crack initiation at high as opposed to low plastic strain amplitude. Previous workers (34) have demonstrated that in aluminum alloys at low strain, cracks tend to be associated with constituent particles. At high strain amplitudes, cracks tend to be associated with slip bands, independent of particles.

If implantation homogenizes slip on the surface, the effect of the implantation should be greatest where crack initiation is associated with slip bands. Scanning electron micrographs of fatigued implanted and unimplanted surfaces (cycled at  $\pm 1.2\%$  total strain) are shown in Figure 15. This amplitude corresponds to the high strain region of the Coffin-Manson plot. The unimplanted surface shows very coarse slip bands. The implanted surface shows almost no features indicating implantation induced much more homogeneous slip. Implantation

improves the low cycle fatigue (LCF) of underaged 7475 in a commercially processed (partially recrystallized) condition at high strain amplitudes ( $> .001$  plastic strain amplitude). This is because at these high strain amplitudes fatigue cracks initiate at slip bands in the unimplanted condition. Implantation homogenizes slip at the surface thus increasing the number of cycles to initiate cracks. In addition, implantation changes the fatigue crack initiation mechanism (FCI) from slip bands to grain boundaries. The initiation site changes because the implanted particles disperse slip so effectively within the grains that the next site of strain incompatibility become grain boundaries. Therefore crack initiation at grain boundaries become the dominant mechanism. At low strain amplitudes implantation did not improve the LCF life because fatigue tended to be associated with constituent particles. Since this is an internal rather than a surface mechanism, implantation did not affect FCI at low strain amplitudes.

There are several important differences between the implanted and unimplanted alloys with respect to cyclic stress-strain behavior. In the implanted alloy, the saturation region (stable hysteresis loop) lasts much longer before tensile load drop and final failure. In the nonimplanted alloy, the saturation region lasts a much shorter number of cycles. Figure 16 is a plot of plastic strain amplitude against number of cycles at constant total strain in the implanted and unimplanted conditions. Both exhibit cyclic hardening (as shown by decreasing plastic strain) but plastic strain reaches stability or saturation in the implanted case after repeated cycling whereas in the unimplanted case saturation last a fewer number of cycles. Also, at a given number of cycles, plastic strain is lower in the unimplanted case.

This indicates that "damage" is more reversible and slip more homogeneous in the implanted condition. This in turn results in the ability to achieve a long stable saturation stress before the initiation of cracks.

Ion implantation had no effect on the LCF life of ITMT 7475 as shown in Figure 17. This is due to the fact that at all strain amplitudes FCI mechanisms are internal ones. At high strain amplitudes, cracks initiate at grain boundaries in both the implanted and unimplanted conditions. Figure 18 shows scanning electron micrographs of these grain boundary cracks on the surface of specimens *just below the fracture surface*. This specimen was cycled at a strain amplitude of  $\pm 1.2\%$ . Figure 19 are replicas of the surface of a specimen cycled at  $\pm 1.2\%$  strain amplitude to approximately half life, and shows slip bands intersecting a grain boundary and mismatch of slip bands across a grain boundary. We have previously shown that grain boundary cracking is enhanced when the material has a random texture (35). The random texture causes the slip length to be determined by grain size. Since the slip bands cannot cross the grain boundaries due to their high misorientation, the grain boundaries become the major point of strain incompatibility. Also grain boundary sliding at room temperature has been demonstrated in aluminum (36) and this might also contribute to grain boundary cracking.

At low strain amplitudes FCI occurred at constituent particles intersected by slip bands. Figure 18 shows optical replicas of a fatigued surface cycled at  $\pm .65\%$  total strain amplitude to approximately half life. The micrographs show fatigue crack initiation at slip band-particle intersections. This mechanism has been found in 2024

aluminum at low stress levels by Kung and Fine (37). In this case it appears that implantation might have no effect on LCF life since the FCI mechanism seems an internal one in the unimplanted condition.

#### Laser Processing .

The studies on the effectiveness and feasibility of rapid surface melting and self-quenching of 2219 Al alloy with continuous wave CO<sub>2</sub> laser have begun. Here the goals are to obtain a surface layer free of large constituent particles which were found so detrimental in the 7475 study. In addition, a considerably hardened layer compared to the bulk may be produced resulting in an enhanced resistance to fatigue, wear and abrasion. The initial studies are focused on the measurements of melt depth, microhardness and documentation of microstructural changes with variations in the laser beam power, surface condition and speed at which the work piece is translated with respect to the laser source.

The 2219 plate was heated by the laser source under two conditions. In the first condition, the plate was surface ground to 5 $\mu$ m finish and in the second the surface was also sand blasted to increase the absorptance of the power. Using both these conditions, 22 runs were made with the beam power of 2, 3, 4 and 5KW and at translation speeds 42, 63, 85, 106 mm/sec. The absorptance in the as-ground conditions is believed to be only 10-20 percent and in the sand-blasted condition to be about 60-80 percent.

Laser melting was accomplished by sweeping the work piece at controlled speeds. When the work piece is swept under the beam a self-quenched heat treated strip or track is obtained along the surface. Normally the dimensions of the width and the depth of the track are

controlled by the power density, beam size and travel speed. In the present course the beam size has been kept constant at 1 mm. Due to the extremely high translational speeds the dwell time of the laser source is approximately 12 milliseconds for each track.

The top view and the side view of the laser tracks have been investigated in a few selected samples. The melt depths range from 0.26 to 0.4 mm with the sand blasted sample at 5 KW and 106 mm/sec traverse speed (sample #22) exhibiting the maximum due to highest power absorption. An optical view of the melt depth for sample #22 is shown in micrograph Figure 19, at 50X SEM examination of the melted and non-melted part of the alloy. Figure 20 shows clearly that there is a great refinement of the microstructure and also the dissolution of the intermetallic constituents suggesting that the temperatures exceeded 1000° C over a period of 12 milliseconds. Similar features were also observed for sample #4 which was only surface ground and processed with 5K watt and 85 mm/sec speed. One of the major differences in samples #4 and #22 is the resulting grain structure. In sample #4, Figure 21a, equiaxed grains were observed near the interface and slightly elongated grains away from the interface. In sample #22, Figure 21b, mostly columnar grains and a region approximately 15 $\mu$ m in size free of any well-defined structure was observed. This is due to a planar solidification front set up during fast quenching. An indepth analysis of these features require estimates of thermal gradients, growth rate (G) and freezing rate (F) in both the samples. It is possible to perform such calculations (38) on the present alloy and will be a subject of investigation in the immediate future.

## PROFESSIONAL PERSONNEL

Dr. E. A. Starke, Jr.

Dr. Kumar Jata

Dr. Wolfgang Ruch

Dr. C. J. Beevers

## GRADUATE STUDENTS

Dwight Janoff

Fred Daus

## PRESENTATIONS AND PUBLICATIONS UNDER AFOSR-83-0061

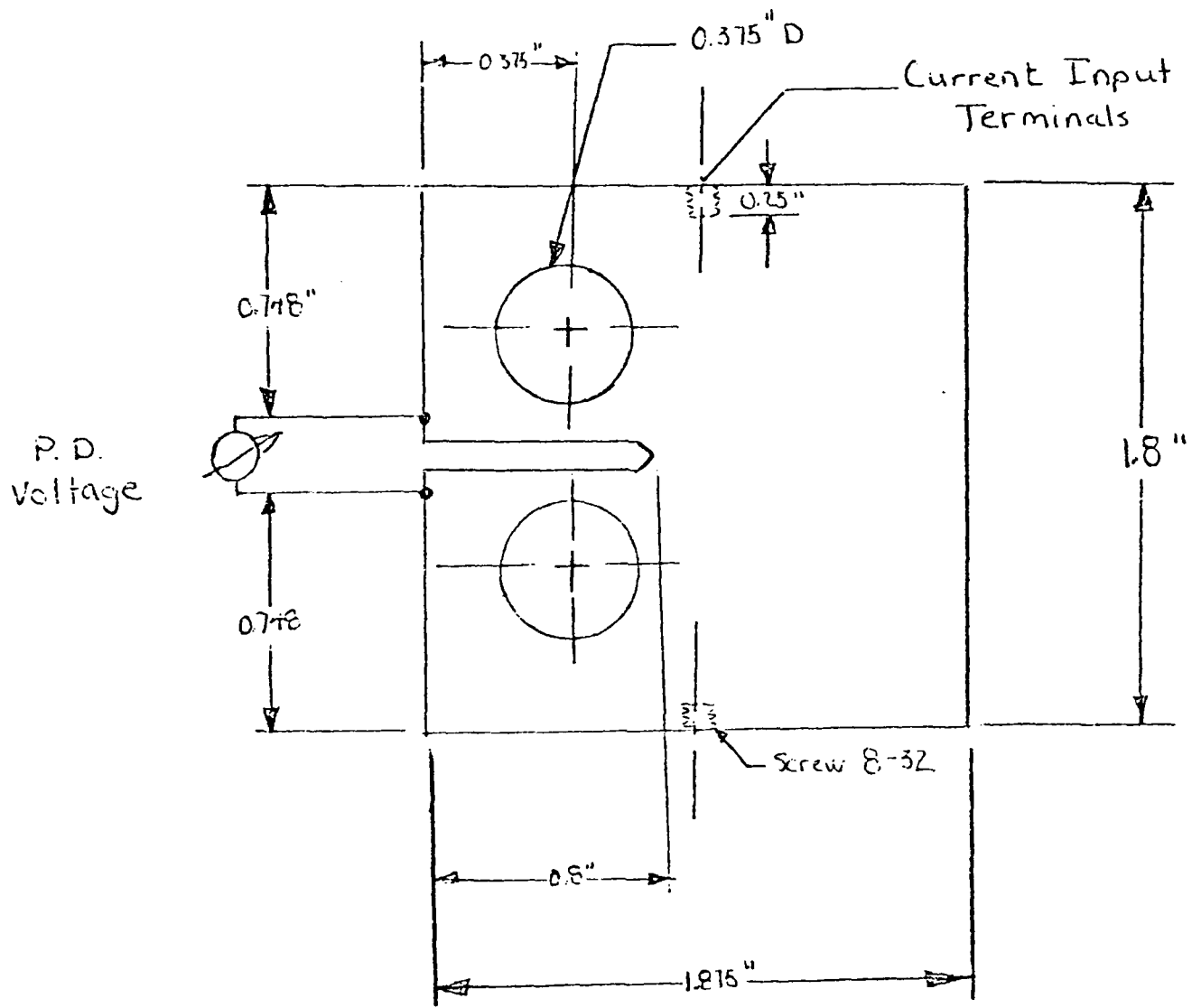
1. R. D. Carter, E. W. Lee, E. A. Starke, Jr. and C. J. Beevers, "The Effect of Microstructure and Environment on the Fatigue Crack Closure of 7475 Aluminum Alloy," Met. Trans. A., Vol. 15A 1984, pp. 555-563.
2. Dwight Janoff and E. A. Starke, Jr., "The Effect of Fe<sup>+</sup> Implantation on the Fatigue Behavior of Alloy 7475," paper presented at the Fall Meeting of the Metallurgical Society of AIME, Detroit, MI, September 18, 1984.
3. K. V. Jata and E. A. Starke, Jr., "Fatigue Crack Growth and Fracture Toughness Behavior of an Al-Li-Cu Alloy," submitted to Met. Trans. A.

## REFERENCES

1. D. T. Cooper and K. A. Clifford, "Fatigue in Machines and Structures-Aircraft," *Fatigue and Microstructure*, ASM, Metals Park, OH, 1979, p. 29.
2. R. D. Carter, E. W. Lee, E. A. Starke, Jr., and C. J. Beevers: *Metall. Trans. A*, 1984, vol. 15A, p. 555.
3. W. S. Miller, A. J. Cornish, A. P. Titchener, and D. A. Bennet: in *Aluminum-Lithium Alloys II*, E. A. Starke, Jr., and T. H. Sanders, Jr., eds., TMS-AIME, Warrendale, PA, p. 355, 1984.
4. T. H. Sanders, Jr., and E. A. Starke, Jr., eds., *Aluminum-Lithium Alloys*, TMS-AIME, 1981.
5. E. A. Starke, Jr., and T. H. Sanders, Jr., eds., *Aluminum-Lithium Alloys II*, TMS-AIME, Warrendale, PA, 1984.
6. W. X. Feng, F. S. Lin, and E. A. Starke, Jr.: *Metall. Trans. A*, 1984, 15, p. 1209.
7. E. A. Starke, Jr., and F. S. Lin: *Metall. Trans. A*, 1982, 13A, p. 2259.
8. T. H. Sanders, Jr., and E. A. Starke, Jr., *Acta Metall.* 1982, 36, p. 927.
9. G. M. Ludtka and D. E. Laughlin: *Metall. Trans. A*, 1981, p. 2083.
10. E. Hornbogen, and K. H. Zum Gahr: *Metallography*, 1975, vol. 8, p. 181.
11. H. Gleiter and E. Hornbogen: *Phys. Status, Solidi.*, 1964, 12, p. 235.
12. H. Gleiter and E. Hornbogen: *Mater. Sci. Eng.*, 1967/68, 2, p. 285.
13. C. J. Beevers: in *Fatigue Thresholds, Fundamentals and Engineering Applications*, J. Backlund, A. F. Blom, and C. J. Beevers, eds., *Engineering Materials Advisory Services, Ltd.*, West Midlands, UK, 1981, Vol. 1, p. 257.
14. R. L. Donahue, H. M. Clarke, P. Alonano, R. Kumble, and A. J. McEvily: *Inter. J. of Fract. Mech.*, 1972, 8, p. 209.
15. A. K. Vasudevan, P. E. Bretz, A. C. Miller, and S. Suresh: *Mater. Sci. and Eng.*, 1984, 64, p. 113.
16. J. Lindigkeit, G. Terlinde, A. Gysler, and G. Lutjering: *Acta Metall.* 1979, vol. 27, p. 1717.

17. E. Hornbogen and K-H. Zum Gahr: *Acta Metall.*, 1976, vol. 24, p. 581.
18. S. Suresh: *Metall. Trans.*, 1983, vol. 14A, p. 2375.
19. E. A. Starke, Jr., T. H. Sanders, Jr., and I. G. Palmer: *Jr. of Metals*, 1981 vol. 33, No. 8, p. 24.
20. F. S. Lin, S. B. Chakraborty and E. A. Starke, Jr.: *Metall. Trans. A*, 1982, 13A, p. 401.
21. J. M. Silcock, T. J. Heal and H. K. Hardy: *J. Inst. of Met.*, 1955-56, 84, p. 23.
22. J. D. Boyd and R. B. Nicholson: *Acta Met.* 1971, 19, p. 1979.
23. J. T. Staley: *Properties Related to Fracture Toughness*, W. R. Warke, V. Weiss and G. T. Hahn, eds., ASTM STP 605, ASTM 1975, p. 71.
24. S. J. Haris, K. Dinsdale, B. Noble: in *Al-Li Alloys II*, E. A. Starke, Jr., and T. H. Sanders, Jr., eds., TMS-AIME, Warrendale, PA.
25. G. G. Garret, and J. F. Knott: *Metall. Trans. A.*, 1978, vol. 9A, p. 1187.
26. G. T. Hahn and A. R. Rosenfield: *Metall. Trans. A*, 1975, 6A, p. 653.
27. J. G. Rinker, M. Marek and T. H. Sanders, Jr.: in *Aluminum-Lithium Alloys*, E. A. Starke, Jr., and T. H. Sanders, Jr., eds. TMS-AIME, Warrendale, PA, p. 597, 1984.
28. E. Smith, T. S. Cook and C. A. Rau: *Fracture*, Proc. 4th Int. Conf. on Fracture (ICF4), D.M.R. Taplin, ed., University of Waterloo Press, Waterloo, Canada, 1977, vol. 1, p. 215.
29. Johanness Weertman: in *Fatigue and Microstructure*, M. Meshii, ed. American Society for Metals, Metals Park, Ohio, 1979, p. 279.
30. J. F. Knott: in *Fundamentals of Fracture Mechanics*, Butterworths & Co. (Publishers) Ltd. London, UK, 1973.
31. R. O. Ritchie and A. W. Thompson: *Metall. Trans. A*, 1985, 16A, p. 233.
32. R. O. Ritchie, W. L. Server and R. A. Wullaert: *Metall. Trans. A*, 1979, 10A, p. 1557.
33. P. Sigmund: *Appl. Phys. Letters*, 25, No. 3, 1974.
34. C. Y. Kung, Ph.D., Thesis, Northwestern University, 1978.

35. Victor W. C Kuo and E. A. Starke, Jr., "The Development of Two Texture Variants and Their Effect on the Mechanical Behavior of a High Strength P/M Aluminum Alloy, X7091," Met. Trans. A, (in press).
36. U. Dahmen and E. Hornbogen: Z. Metallkde, 1975, p. 236.
37. C. Y. Kung and M. E. Fine: Met. Trans. A, 1979, vol. 10A, p. 603.
38. M. C. Flemings, "Solidification Processing," McGraw Hill, NY, 1974.



8-32 Screw and Washer

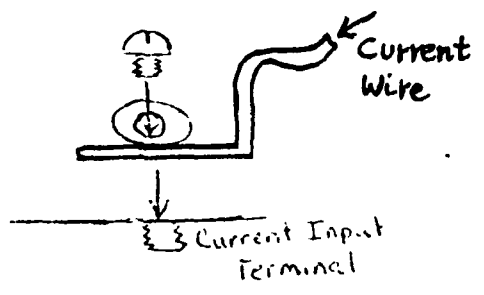


Figure 1: Compact Tension Specimen Design  
Specimen Thickness .3 in.

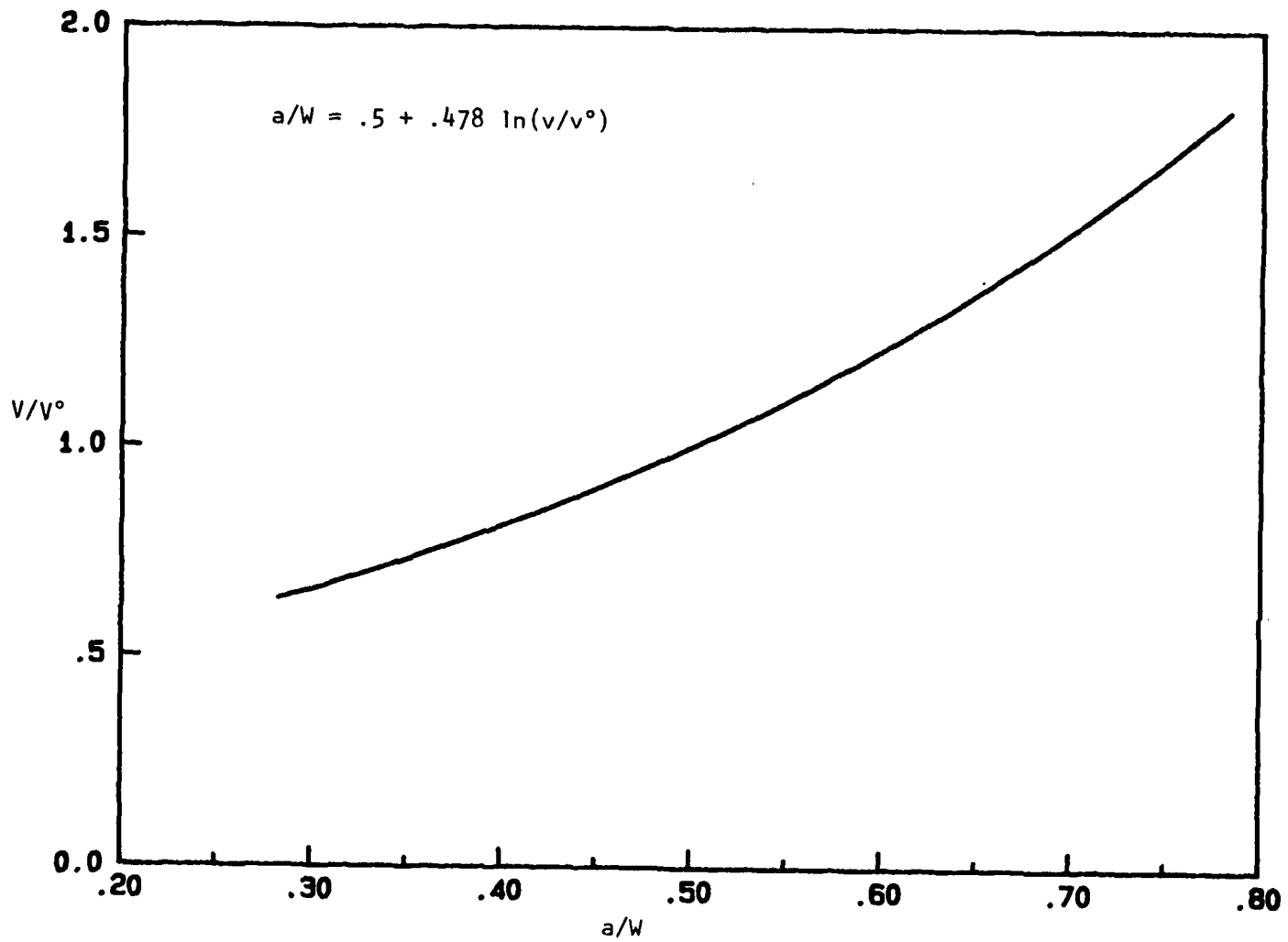


Figure 2: Potential Drop Calibration Curve

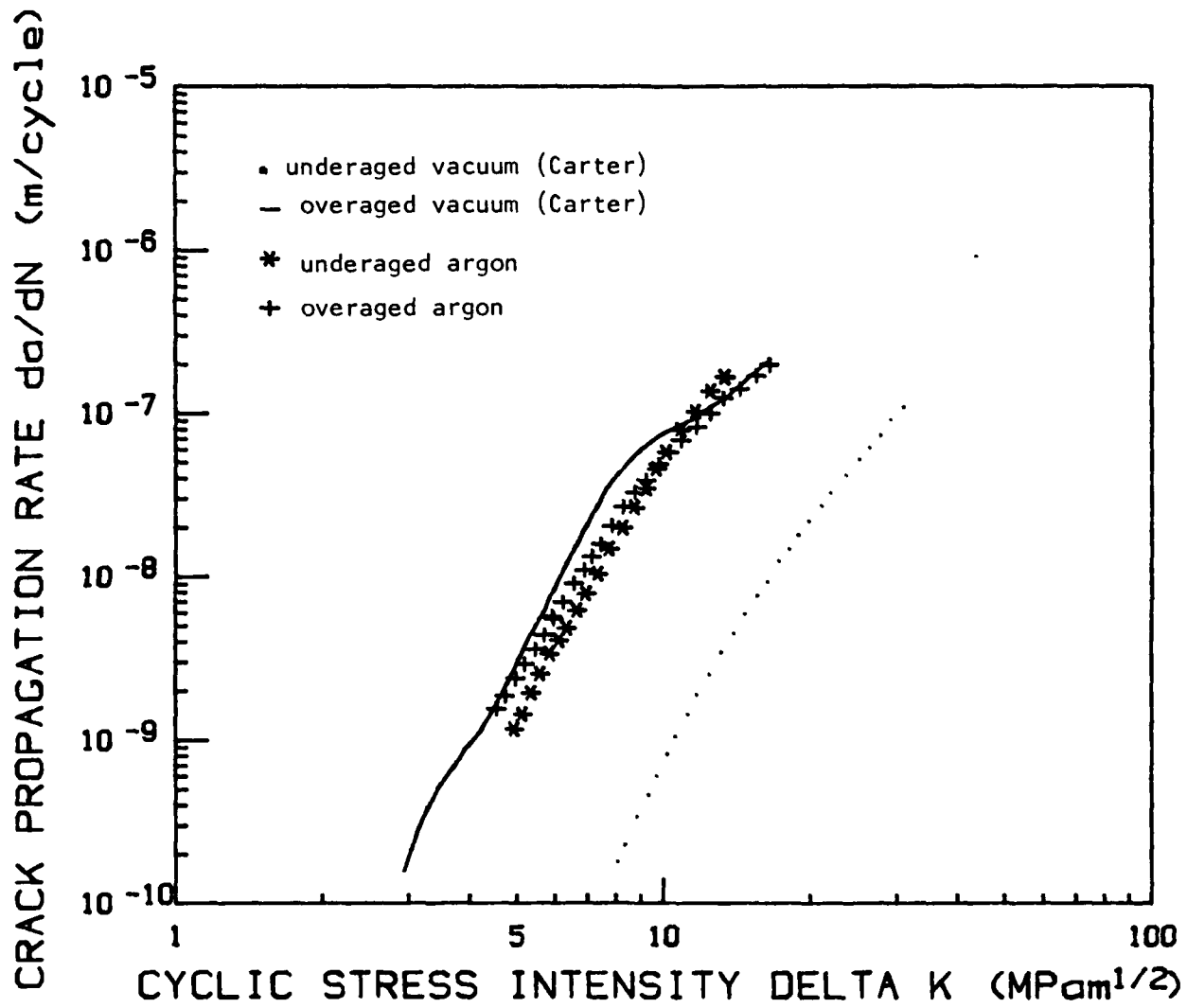


Figure 3: Comparison of Crack Propagation Data

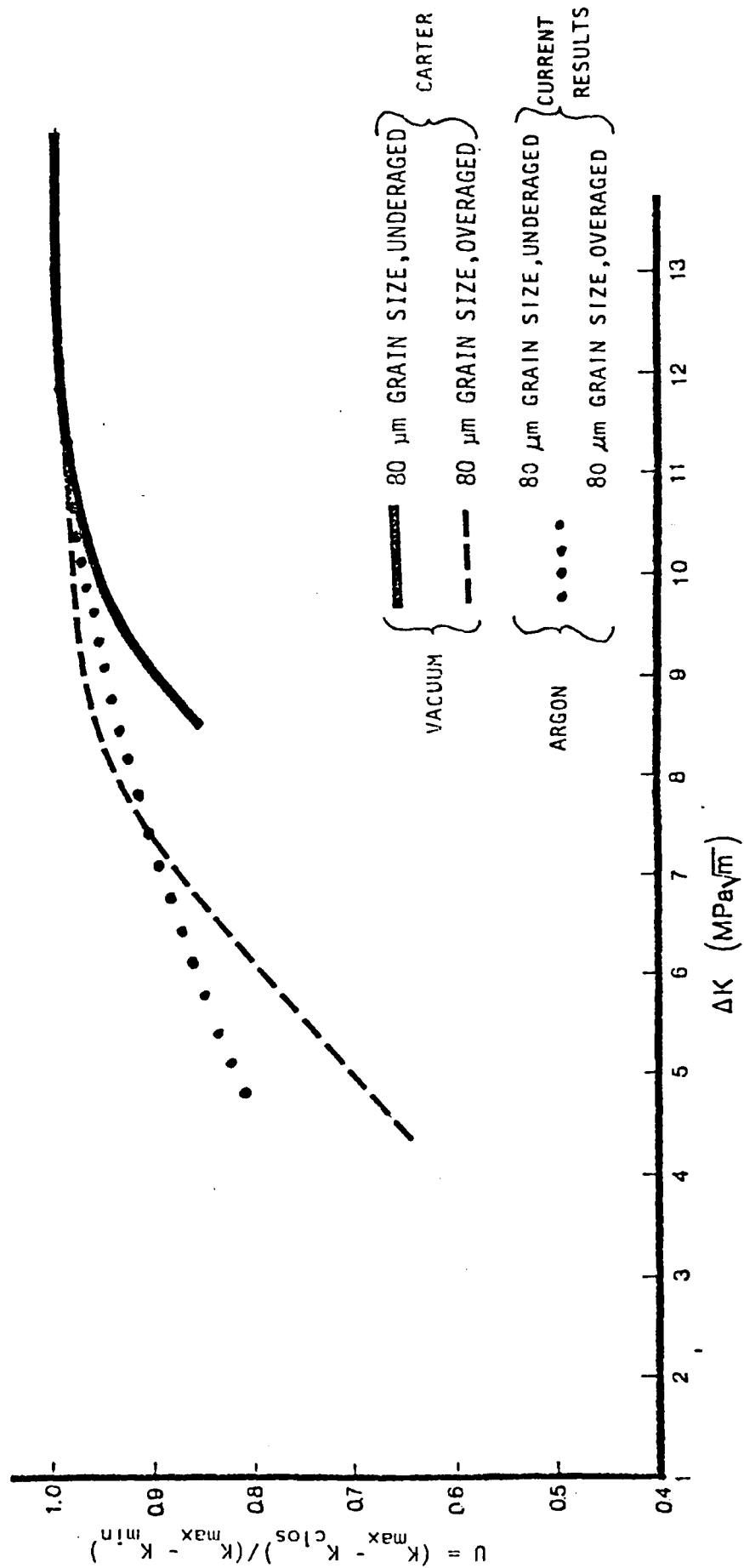
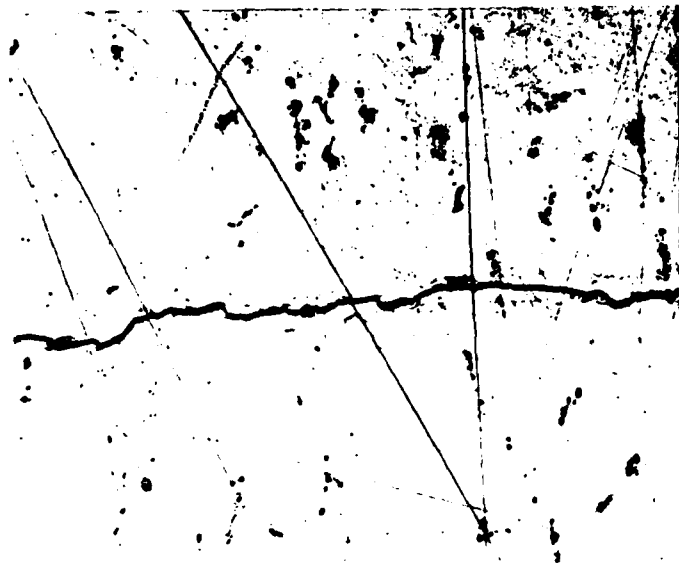
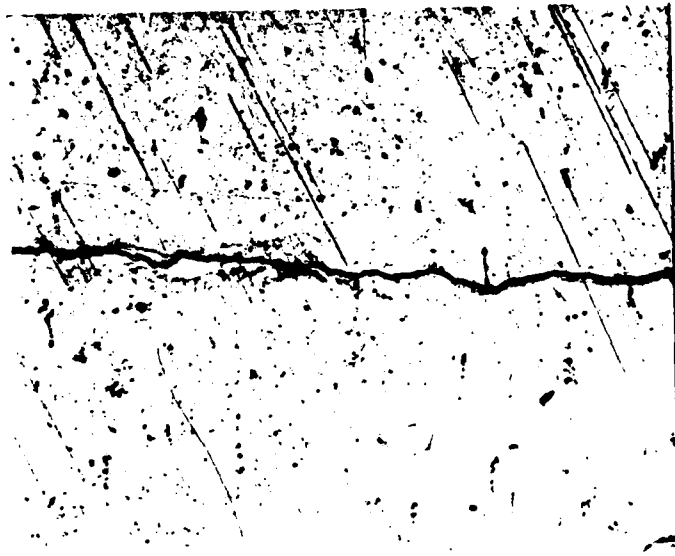


Figure 4: Comparison of Closure Data



a) underaged

500  $\mu\text{m}$



b) overaged

Figure 5: Optical micrographs showing crack paths (+) crack growth direction

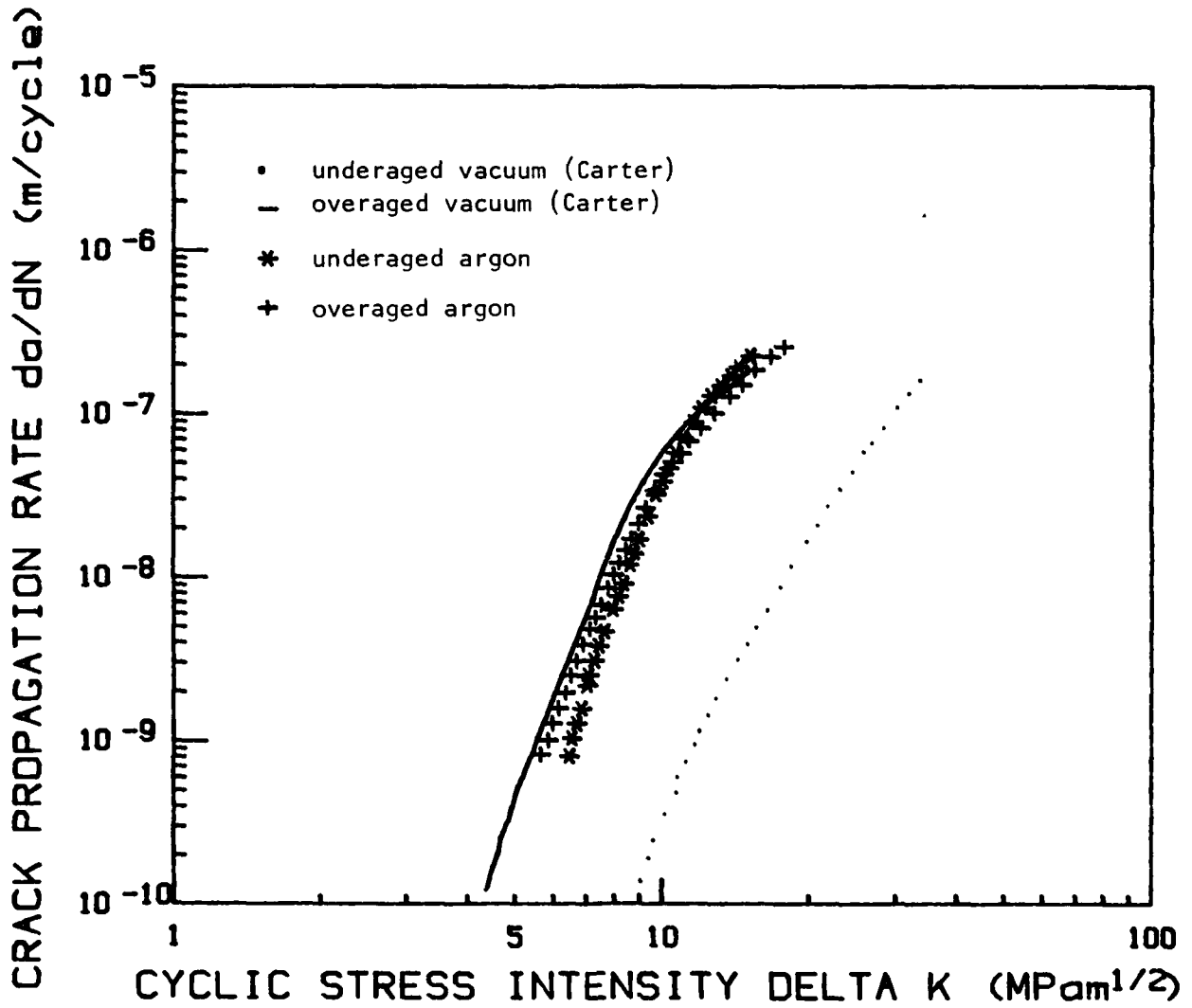


Figure 6: Crack Propagation Curves after Correction for Closure

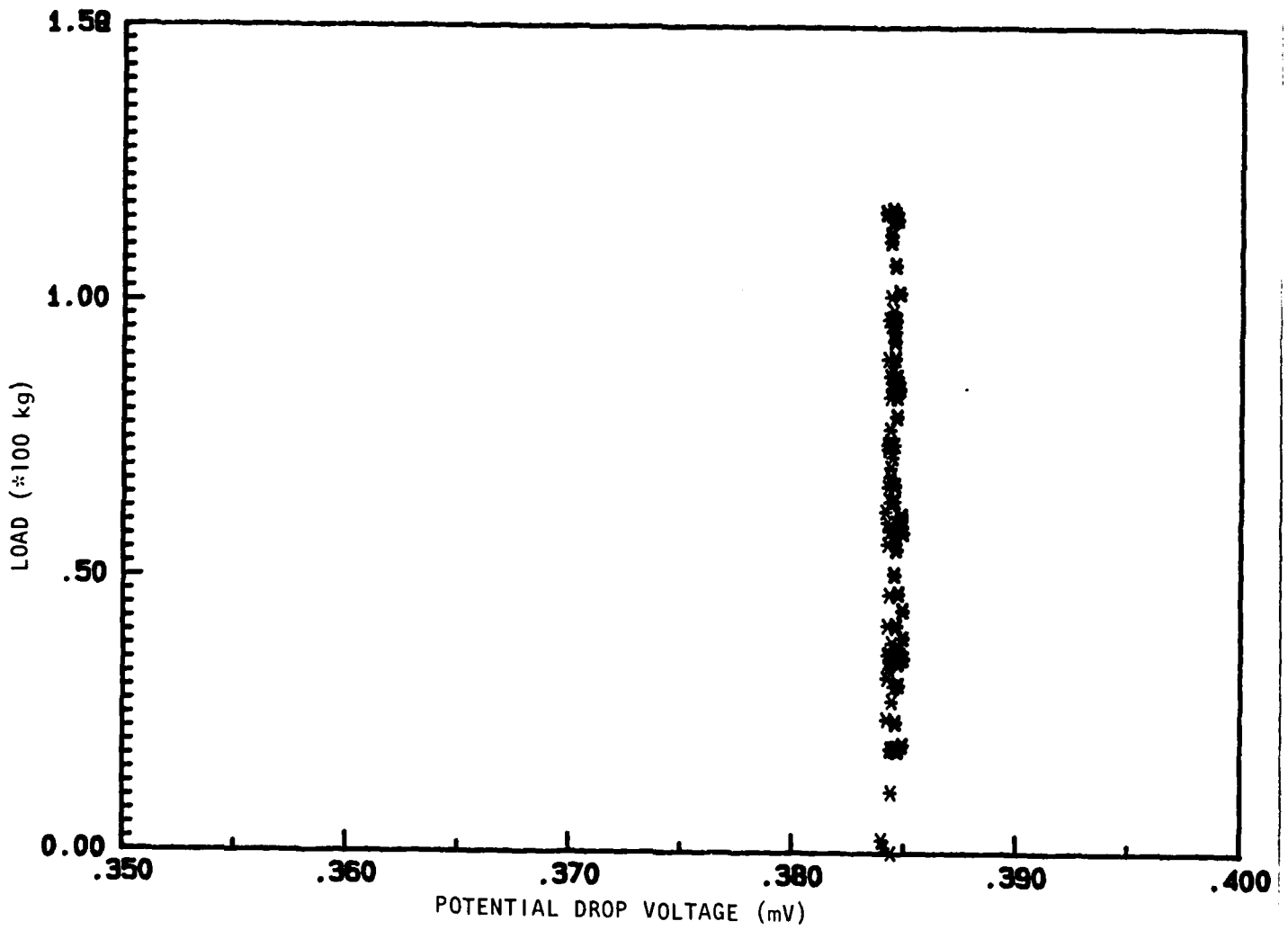


Figure 7: Load - Potential Drop Curve: 7475 underaged, purified argon atmosphere

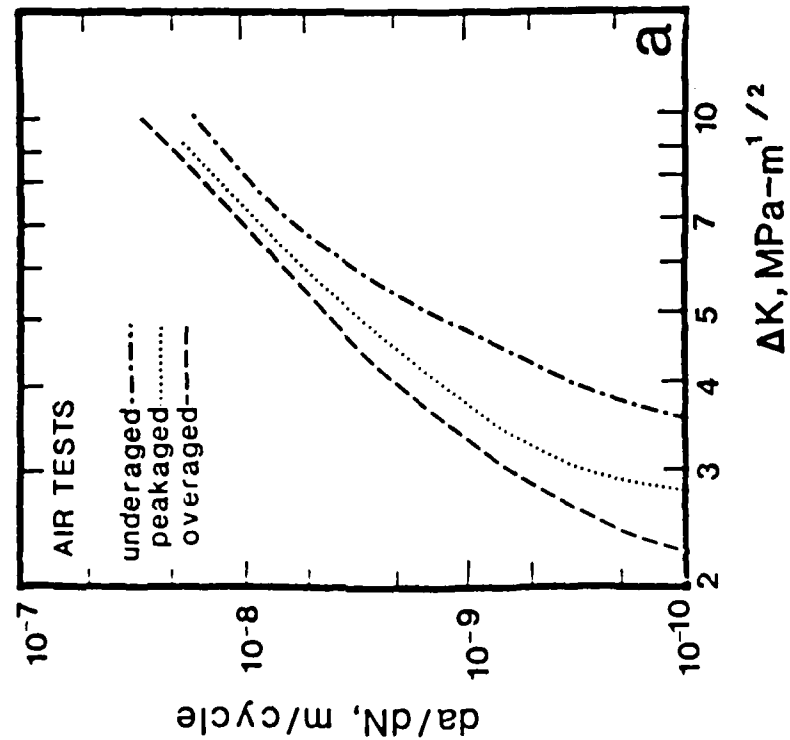
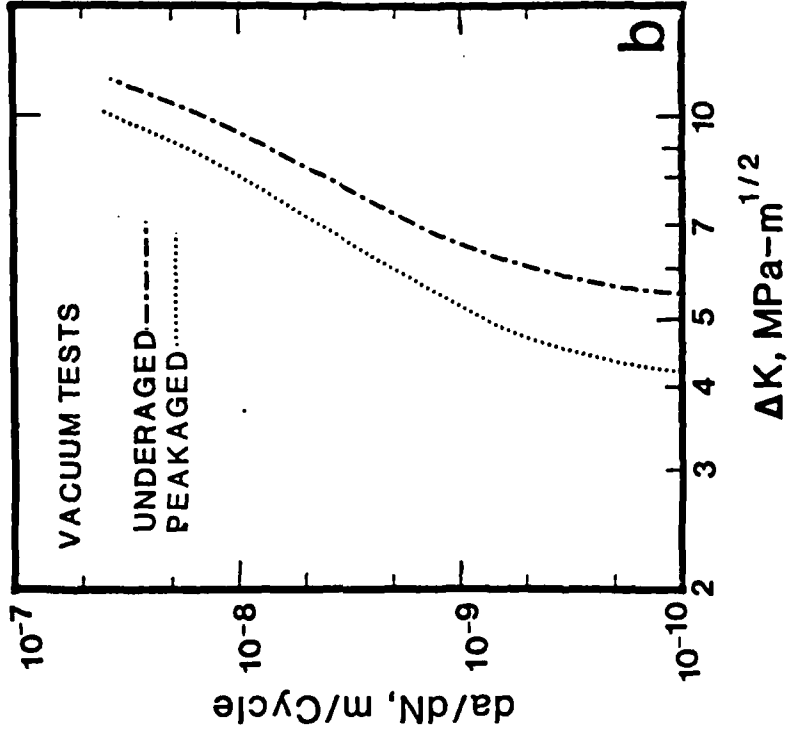


Figure 8: Fatigue crack growth rates of the microstructural variants tested in (a) laboratory air (a R.H. of 45 percent) and (b) vacuum (10<sup>-5</sup> torr)

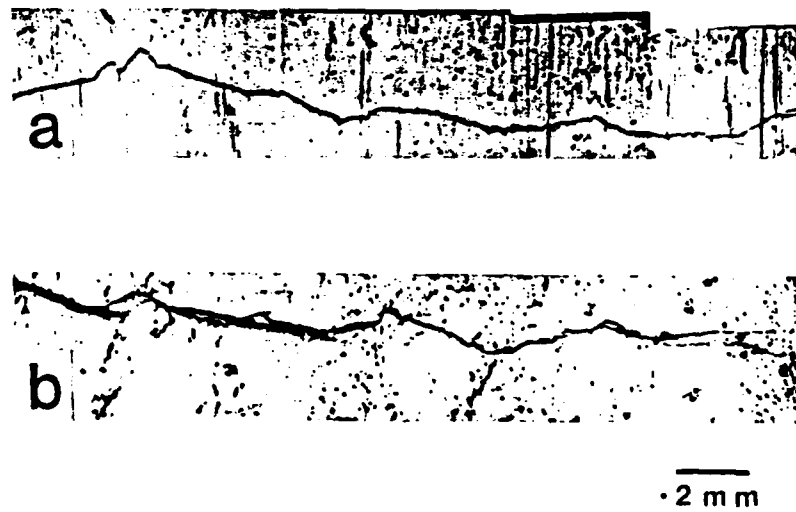


Figure 9: Optical micrographs of the crack profile of the fatigue crack propagation samples tested in air (a) underaged condition and (b) overaged condition

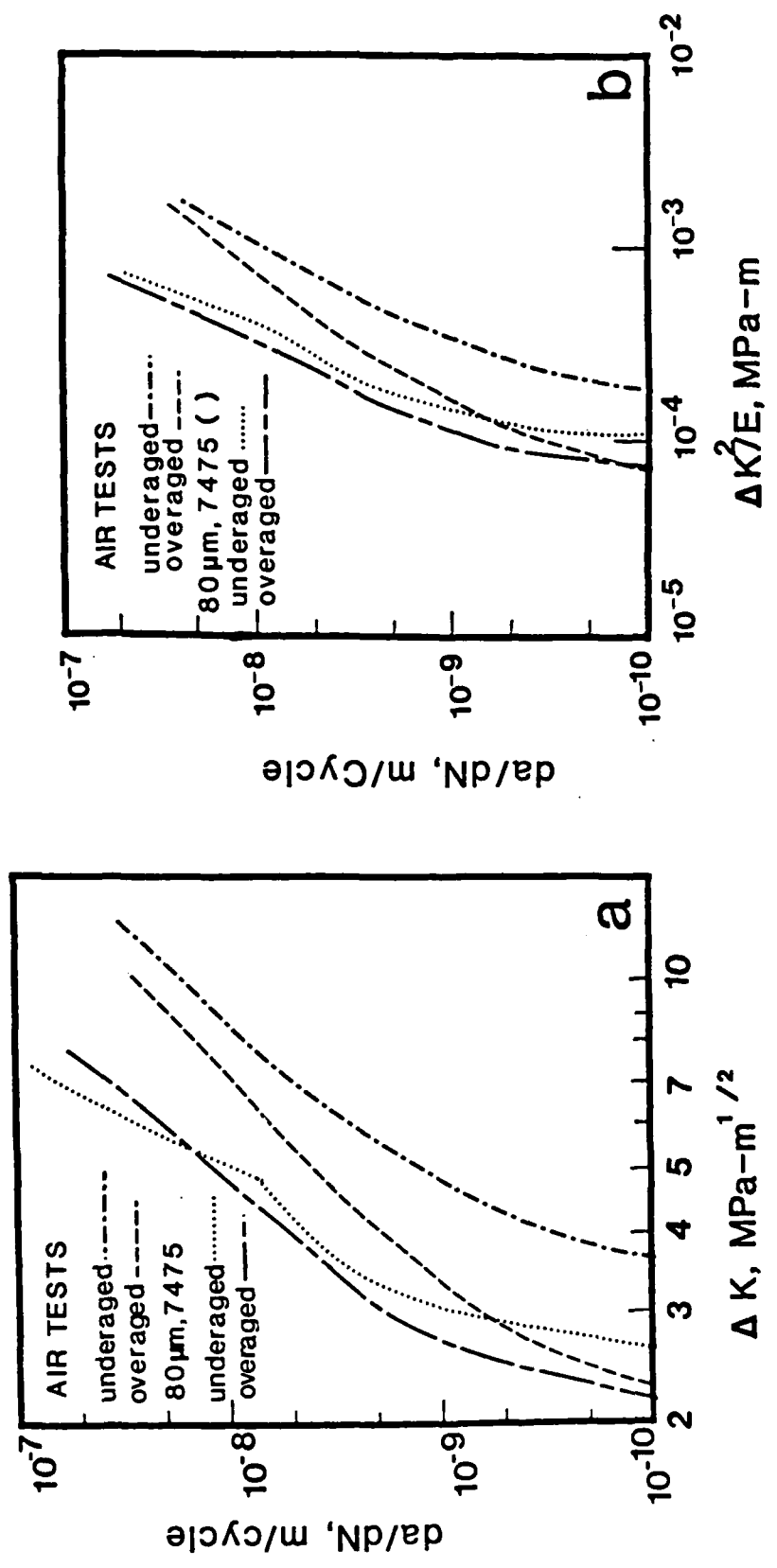


Figure 10: A comparison of the fatigue crack growth rates of the present alloy with thermomechanically processed 7475 alloy as a function of  $\Delta K$  in (a) and as a function of normalized  $\Delta K^2$  with respect to Young's modulus  $E$ , (b)

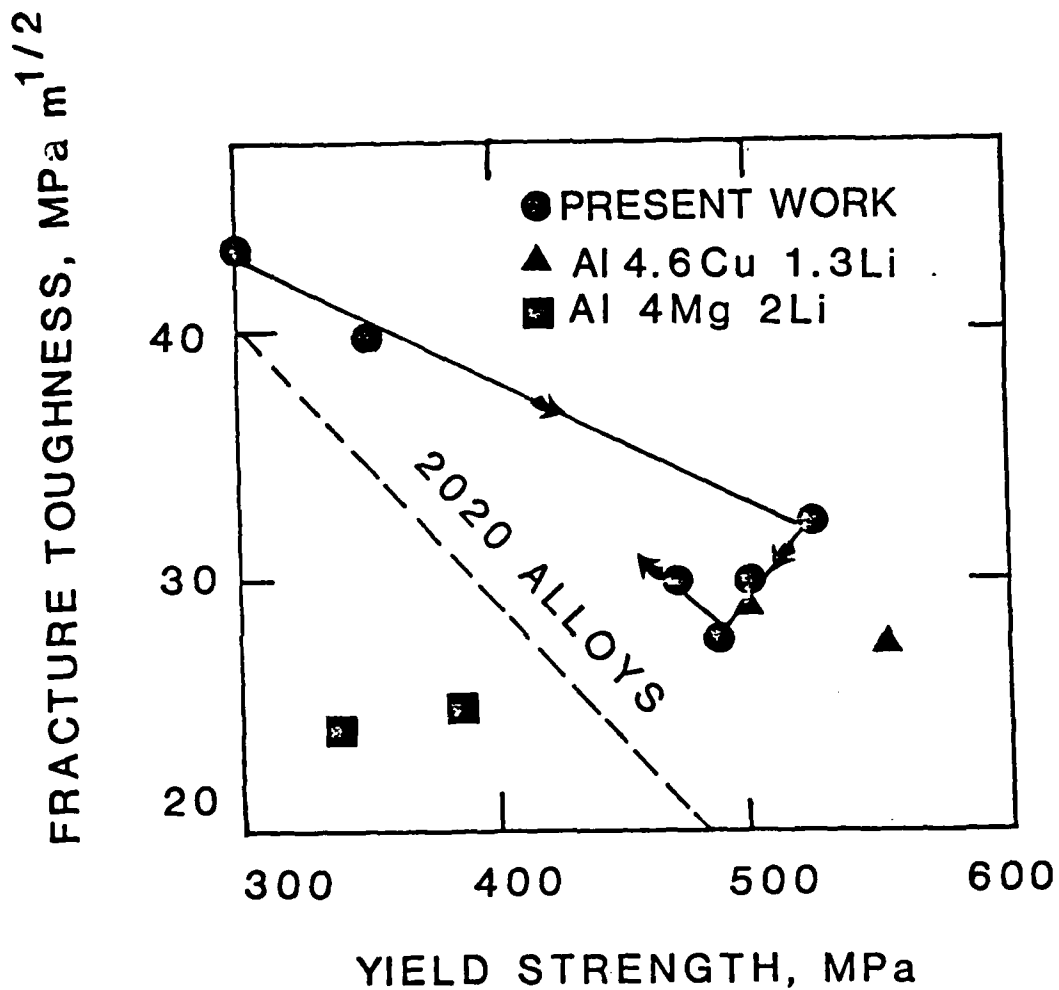
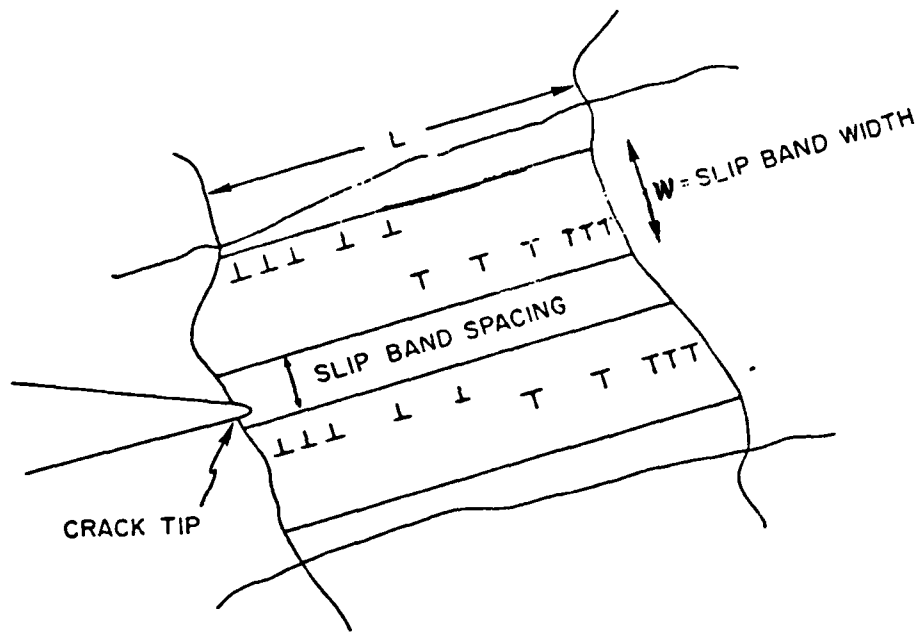
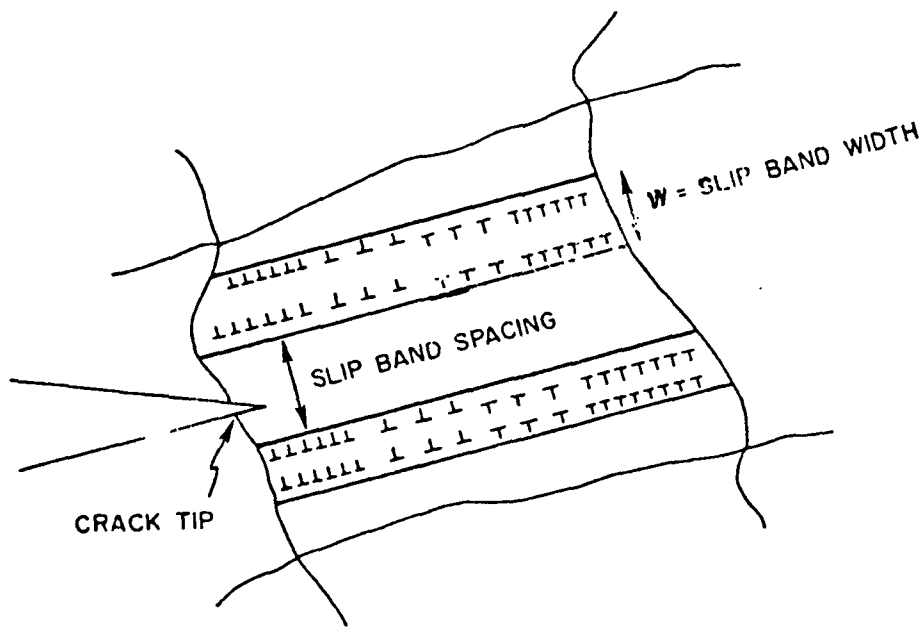


Figure 11: Variation of fracture toughness,  $K_{1C}$ , with yield strength for the present alloy and a comparison to the data of other Al-Li-X alloys



(a) UNDERAGED



(b) PEAKAGED

Figure 12: Schematic illustrating that the slip band developed in front of the crack tip is wider in the (a) underaged condition due to less heterogeneous slip character as compared to the (b) condition

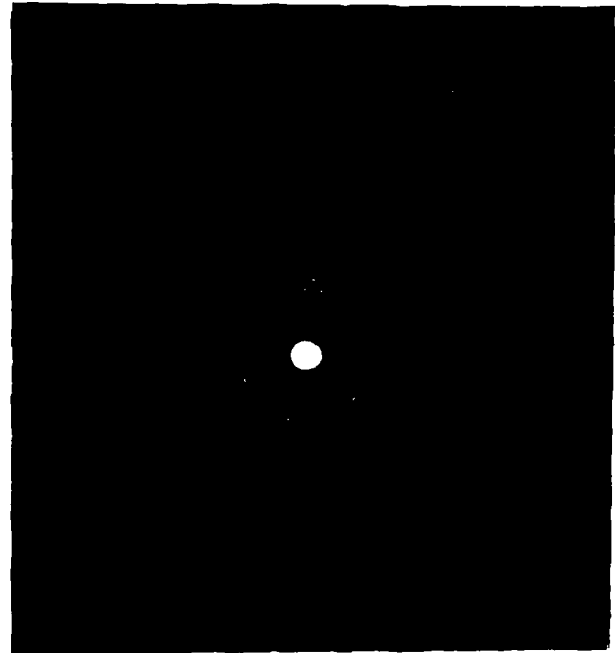


Figure 13: (a) Bright field of implanted surface; arrows show  $\text{Al}_6\text{Fe}$  particles;  
(b) Corresponding ring pattern of  $\text{Al}_6\text{Fe}$

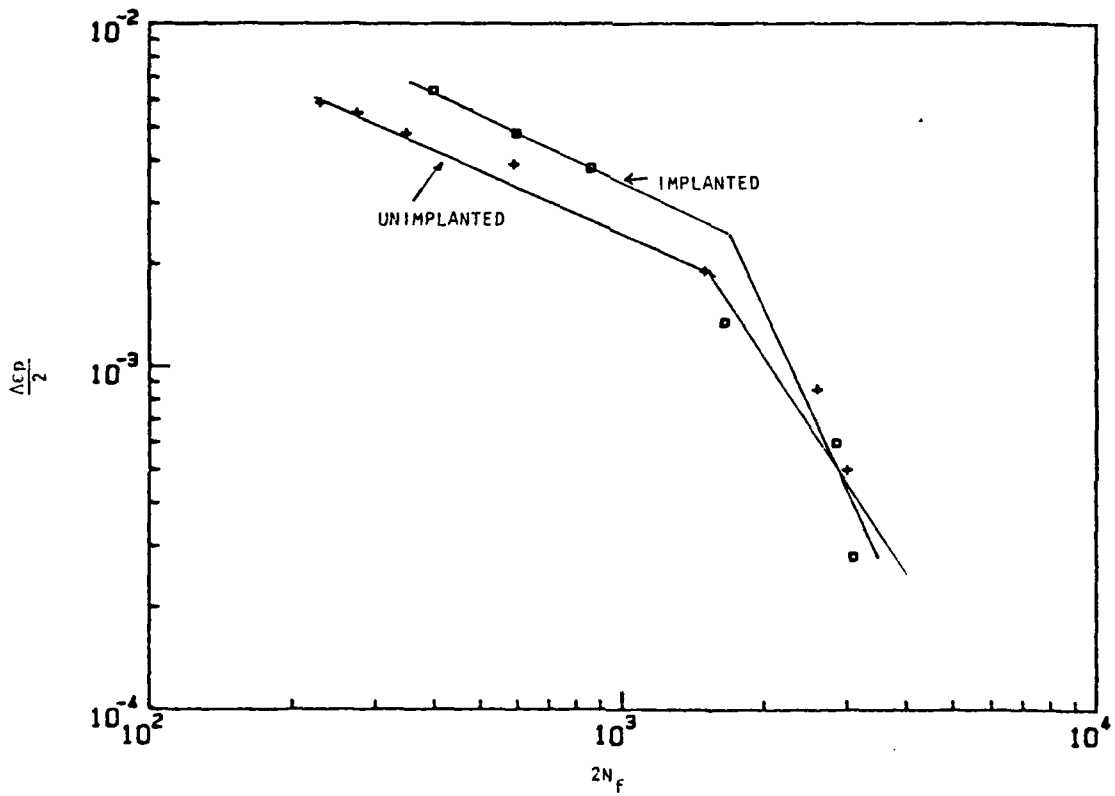
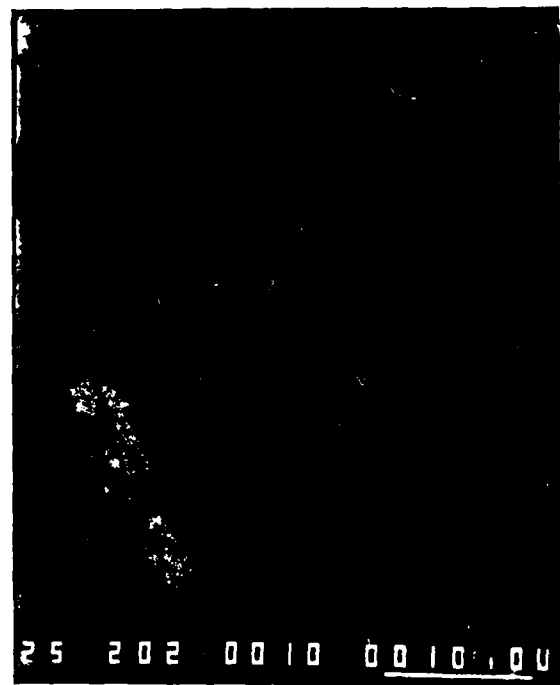


Figure 14: Coffin-Manson plot for the commercial 7475 alloy



3 μm



5 μm

Figure 15: (a) Unimplanted alloy surface, fatigued  $\pm 1.2\%$  strain to failure, stress axis is vertical; (b) Implanted alloy, fatigued  $\pm 1.2\%$  total strain to failure, stress axis is vertical (commercial alloy)

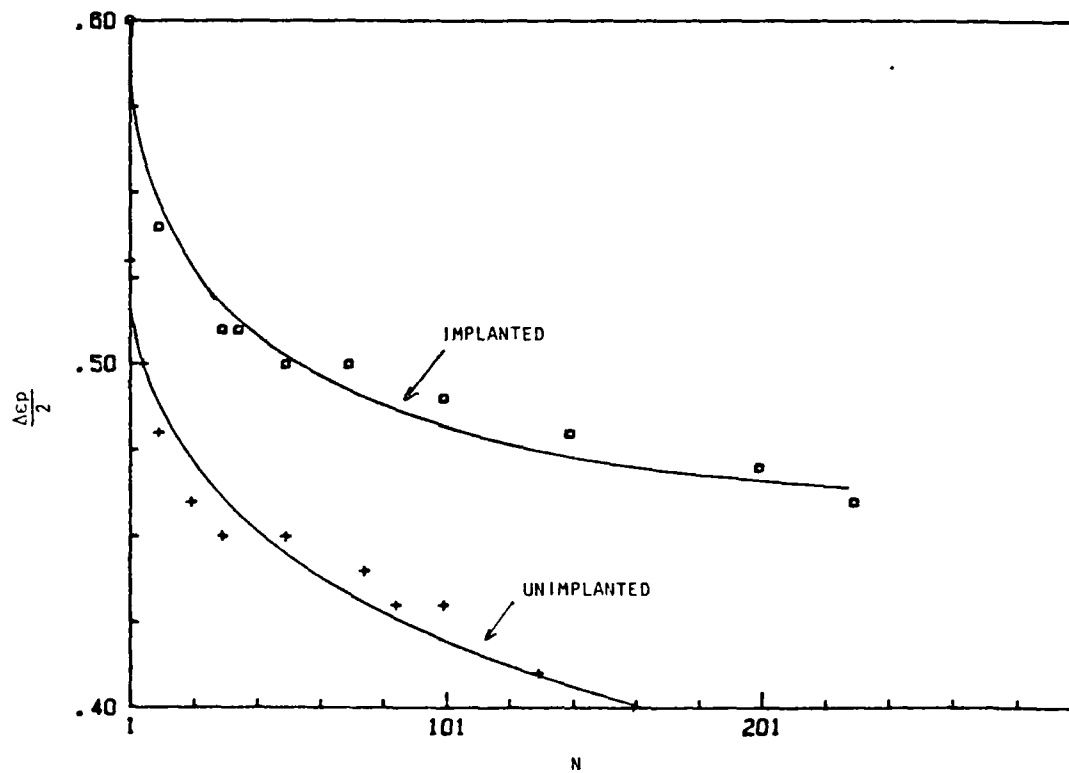


Figure 16: Variation of plastic strain amplitude with cycling for the commercial 7475 alloy ( $\Delta \epsilon_T = \pm 1.2\%$ )

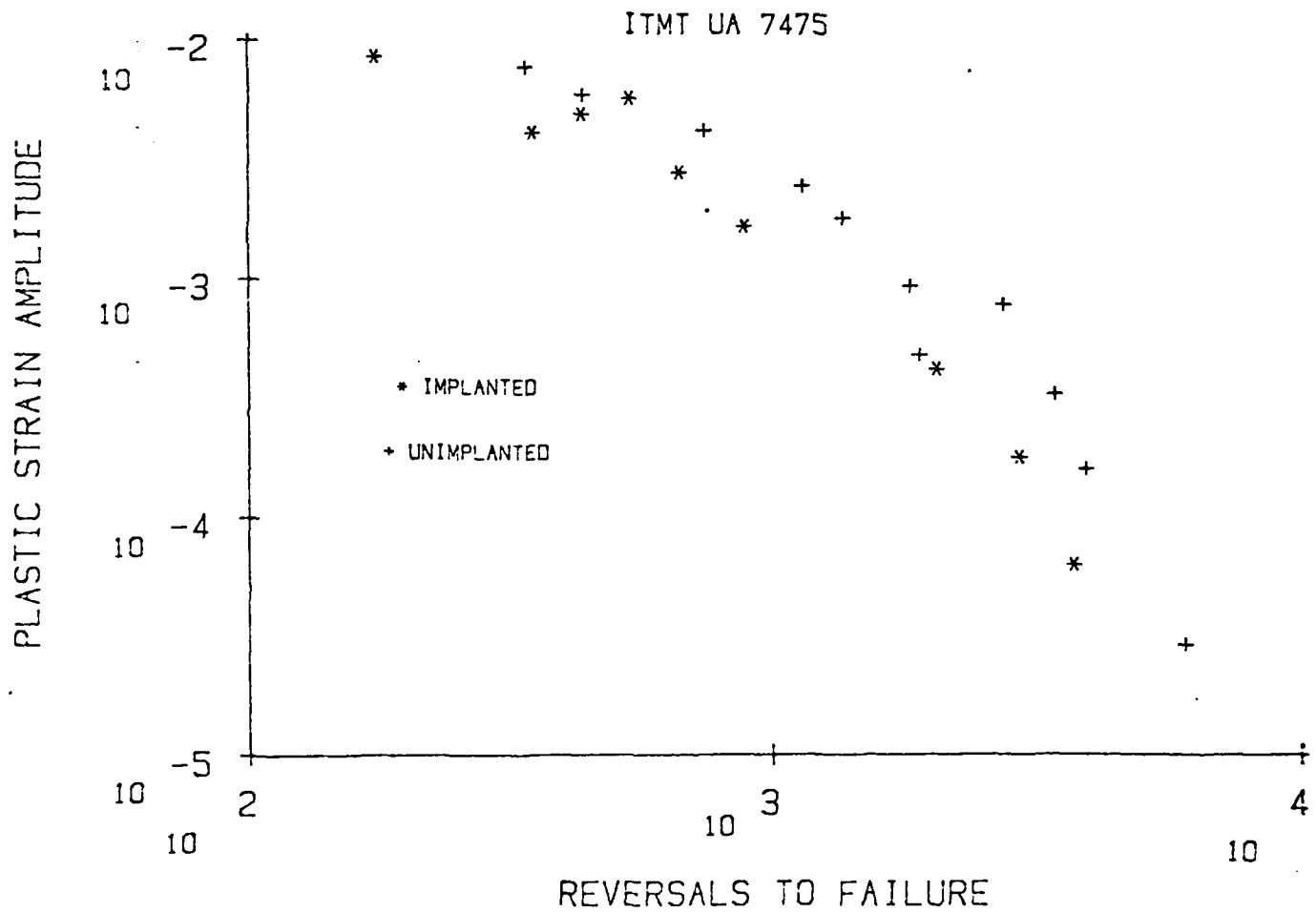


Figure 17: Coffin-Manson plot of implanted and unimplanted UAITMT 7475

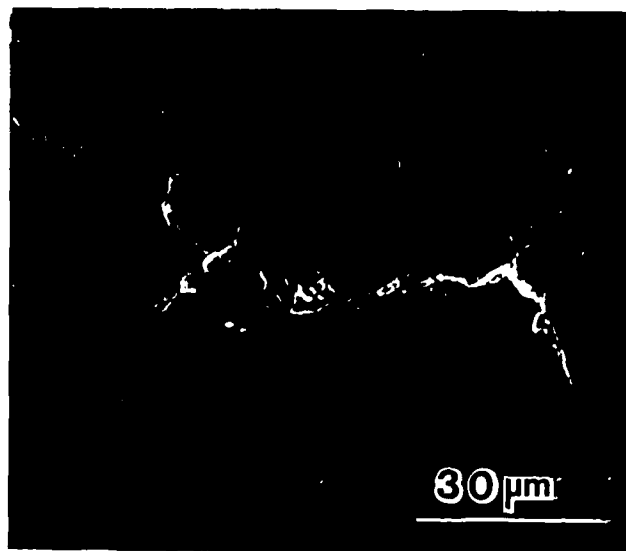
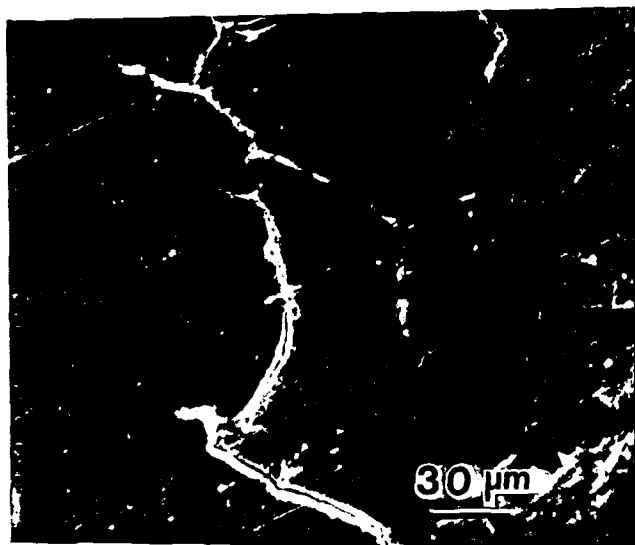
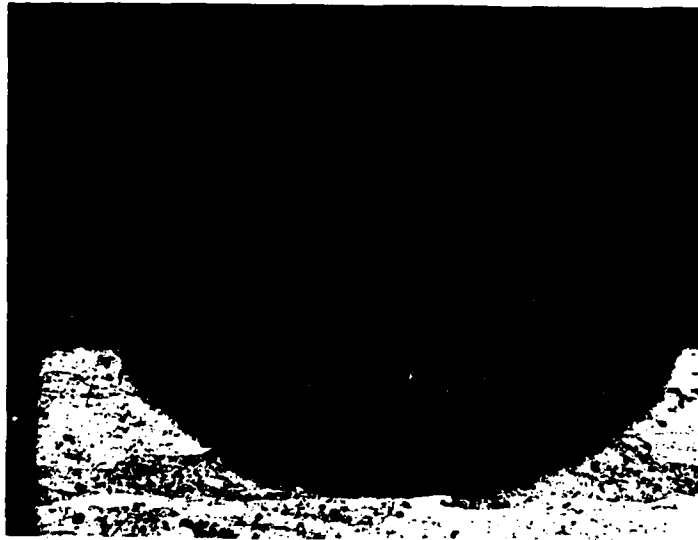
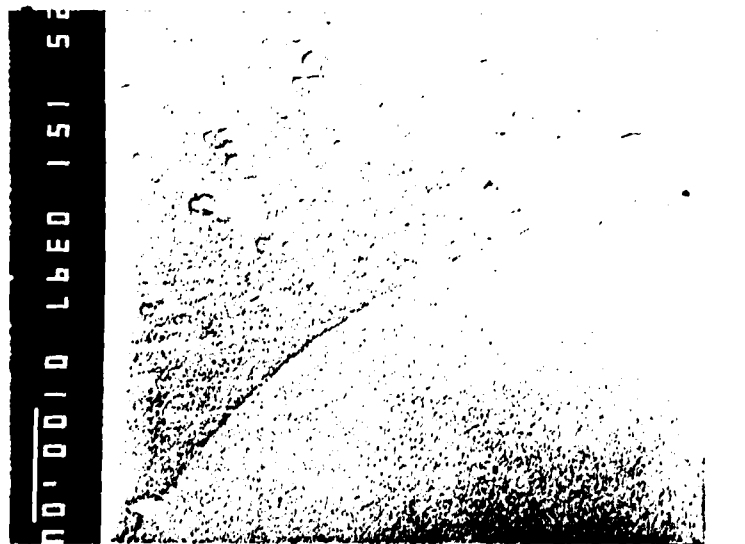


Figure 18: SEMs showing grain boundary cracking in both (a) unimplanted and (b) implanted conditions in a specimen cycled to fracture at  $\pm 1.2\%$  total strain amplitude



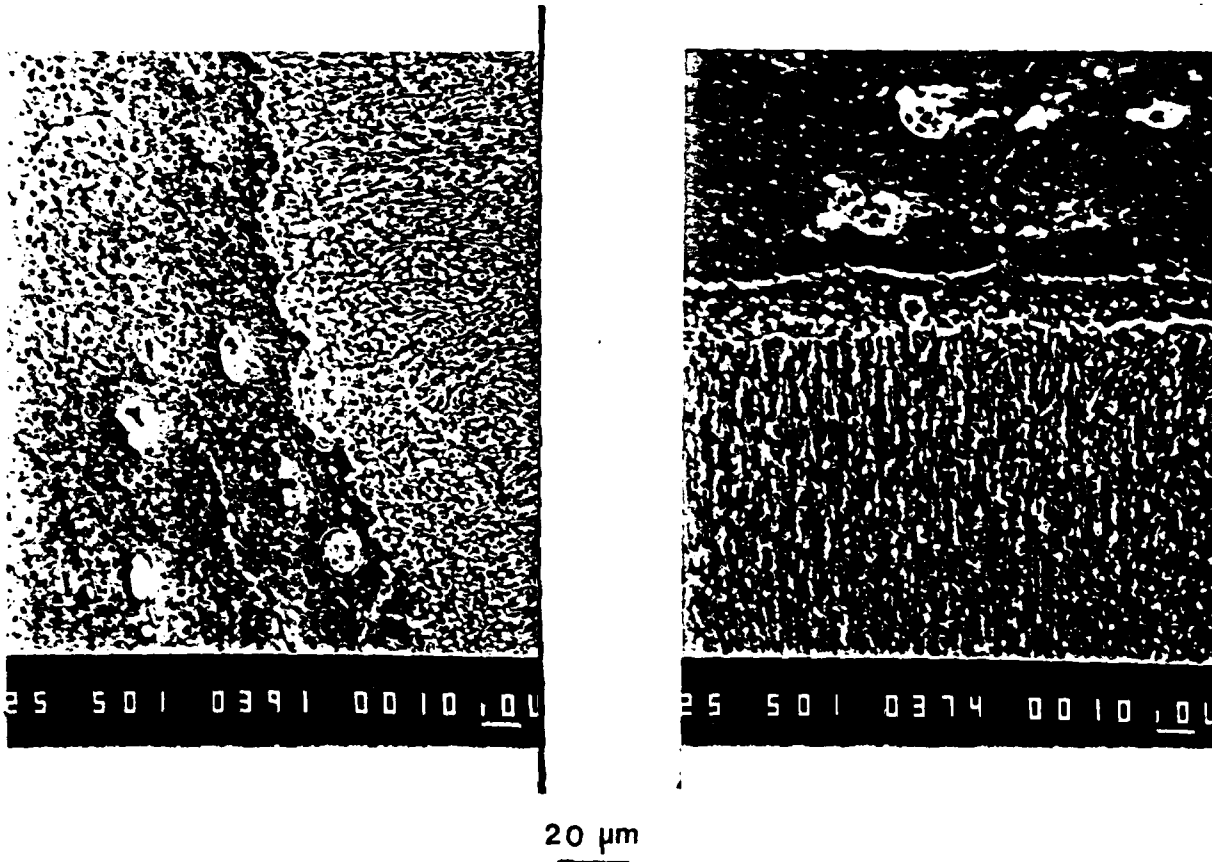
200  $\mu$ m

Figure 19: Optical view (50X) of the melt depth in sample #22 which has been sand blasted prior to laser treatment.  
Conditions (a) Traverse speed 63 mm/sec.  
(b) Beam power 5 kilowatt



100 μm

Figure 20: SEM (150X) showing the refinement in the microstructure in the laser melt of sample #4.  
Conditions (a) Surface not sand blasted  
(b) Traverse speed 85 mm/sec.  
(c) Beam Power 5 kilowatt



DISTRIBUTION LIST

Copy No.

- 1 - 6      Air Force Office of Scientific Research/NE  
            Building 410  
            Bolling Air Force Base  
            Washington, D.C. 20332-6448  
            Attention: Alan H. Rosenstein
- 7 - 8      E. A. Starke, Jr.
- 9 - 10     E. H. Pancake  
            Clark Hall
- 11         SEAS Publications Files

JO#6107:wn

**UNIVERSITY OF VIRGINIA**  
**School of Engineering and Applied Science**

The University of Virginia's School of Engineering and Applied Science has an undergraduate enrollment of approximately 1,500 students with a graduate enrollment of approximately 500. There are 125 faculty members, a majority of whom conduct research in addition to teaching.

Research is a vital part of the educational program and interests parallel academic specialties. These range from the classical engineering disciplines of Chemical, Civil, Electrical, and Mechanical and Aerospace to newer, more specialized fields of Biomedical Engineering, Systems Engineering, Materials Science, Nuclear Engineering and Engineering Physics, Applied Mathematics and Computer Science. Within these disciplines there are well equipped laboratories for conducting highly specialized research. All departments offer the doctorate; Biomedical and Materials Science grant only graduate degrees. In addition, courses in the humanities are offered within the School.

The University of Virginia (which includes approximately 1,500 full-time faculty and a total full-time student enrollment of about 16,000), also offers professional degrees under the schools of Architecture, Law, Medicine, Nursing, Commerce, Business Administration, and Education. In addition, the College of Arts and Sciences houses departments of Mathematics, Physics, Chemistry and others relevant to the engineering research program. The School of Engineering and Applied Science is an integral part of this University community which provides opportunities for interdisciplinary work in pursuit of the basic goals of education, research, and public service.

END

10-86

DTIC